### Title

Dll4 and Notch signalling couples sprouting angiogenesis and artery formation




### Journal

Nature Cell Biology, 19(8)

### ISSN

1465-7392



### Authors

Pitulescu, Mara E
Schmidt, Inga
Giaimo, Benedetto Daniele
et al.



### Publication Date

2017-08-01

### DOI

10.1038/ncb3555

Peer reviewed

nature cell biology

# Dll4 and Notch signalling couples sprouting angiogenesis and artery formation

Mara E. Pitulescu[1,6], Inga Schmidt[1], Benedetto Daniele Giaimo[2], Tobiah Antoine[1], Frank Berkenfeld[1], Francesca Ferrante[2], Hongryeol Park[1], Manuel Ehling[1], Daniel Biljes[1], Susana F. Rocha[1], Urs H. Langen[1], Martin Stehling[3], Takashi Nagasawa[4], Napoleone Ferrara[5], Tilman Borggrefe[2] and Ralf H. Adams[1,6]

**Endothelial sprouting and proliferation are tightly coordinated processes mediating the formation of new blood vessels during physiological and pathological angiogenesis. Endothelial tip cells lead sprouts and are thought to suppress tip-like behaviour in adjacent stalk endothelial cells by activating Notch. Here, we show with genetic experiments in postnatal mice that the level of active Notch signalling is more important than the direct Dll4-mediated cell–cell communication between endothelial cells. We identify endothelial expression of VEGF-A and of the chemokine receptor CXCR4 as key processes controlling Notch-dependent vessel growth. Surprisingly, genetic experiments targeting endothelial tip cells *in vivo* reveal that they retain their function without Dll4 and are also not replaced by adjacent, Dll4-positive cells. Instead, activation of Notch directs tip-derived endothelial cells into developing arteries and thereby establishes that Dll4–Notch signalling couples sprouting angiogenesis and artery formation.**

Angiogenesis is essential during development and regeneration but is also involved in pathological processes such as cancer. Endothelial cell (EC) sprouting and proliferation, which mediate the extension of vascular networks, are induced by tissue-derived vascular endothelial growth factor A (VEGF-A) and its endothelial receptor VEGFR2, also known as Flk1 or KDR[1,2]. Notch signalling interactions between adjacent ECs are thought to coordinate the cooperative behaviour of cells during sprouting angiogenesis. VEGFR2 activity upregulates expression of the Notch ligand Delta-like 4 (Dll4) in filopodia-extending tip cells at the distal end of sprouts[3–5]. In turn, Dll4-mediated activation of Notch suppresses tip cell behaviour in trailing stalk ECs, which form the base of sprouts[3,4,6–8]. Accordingly, inhibition of Dll4–Notch interactions results in excessive sprouting and EC hyperproliferation[3,4,6,8–10]. Dll4–Notch signalling is opposed by the ligand Jagged1, which is pro-angiogenic and predominantly expressed by stalk and capillary ECs[11–13].

The behaviour of sprouting ECs is thought to be highly dynamic, enabling rapid replacement of tip cells and switching between tip/stalk phenotypes[7,14]. Mathematical models have proposed feedback loops involving VEGF-induced Dll4 expression in tip cells and Notch-mediated suppression of VEGFR2 expression in stalk ECs[7,15–18]. Nevertheless, the processes occurring downstream of Notch and the regulation of endothelial sprouting have remained insufficiently understood. Here, we have used genetic and pharmacological approaches in mice to unravel the cooperation between different signalling pathways. Moreover, genetic tools allowing the selective manipulation of tip cells establish that Dll4–Notch signalling induces an endothelial fate switch and specifies future arterial ECs among the tip cell progeny at the angiogenic growth front.

## RESULTS

### Notch-dependent expression of angiogenic regulators

Consistent with previous reports[4,5,8], EC-specific inactivation of the *Dll4* gene in mice (*Dll4*$^{i\Delta EC/\Delta EC}$) at postnatal day 6 (P6) led to a dramatic increase in retinal vessel density with an accompanying loss of arteriovenous patterning (Fig. 1a,b). This phenotype was not enhanced by the simultaneous inactivation of *Dll1*, the gene encoding Delta-like 1, a Notch ligand with limited expression in ECs[19,20] (Supplementary Fig. 1a,b). Arguing that a sufficient threshold of Notch activation is more critical than the actual Dll4-mediated communication between ECs, Cre-dependent expression of active Notch1 intracellular domain (*NICD*$^{iOEC}$) was sufficient to

[1]Max Planck Institute for Molecular Biomedicine, Department of Tissue Morphogenesis, and University of Münster, Faculty of Medicine, Röntgenstrasse 20, D-48149 Münster, Germany. [2]Institute of Biochemistry, University of Giessen, Friedrichstrasse 24, D-35392 Giessen, Germany. [3]Max Planck Institute for Molecular Biomedicine, Flow Cytometry Unit, Röntgenstrasse 20, D-48149 Münster, Germany. [4]Laboratory of Stem Cell Biology and Developmental Immunology, Graduate School of Frontier Biosciences and Graduate School of Medicine, Osaka University, 1-3 Yamada-oka, Suita, Osaka 565-0871, Japan. [5]University of California San Diego Medical Center, 9500 Gilman Drive, La Jolla, California 92093, USA.
[6]Correspondence should be addressed to M.E.P. or R.H.A. (e-mail: mara.pitulescu@mpi-muenster.mpg.de or ralf.adams@mpi-muenster.mpg.de)

Received 4 May 2016; accepted 15 May 2017; published online 17 July 2017; DOI: 10.1038/ncb3555

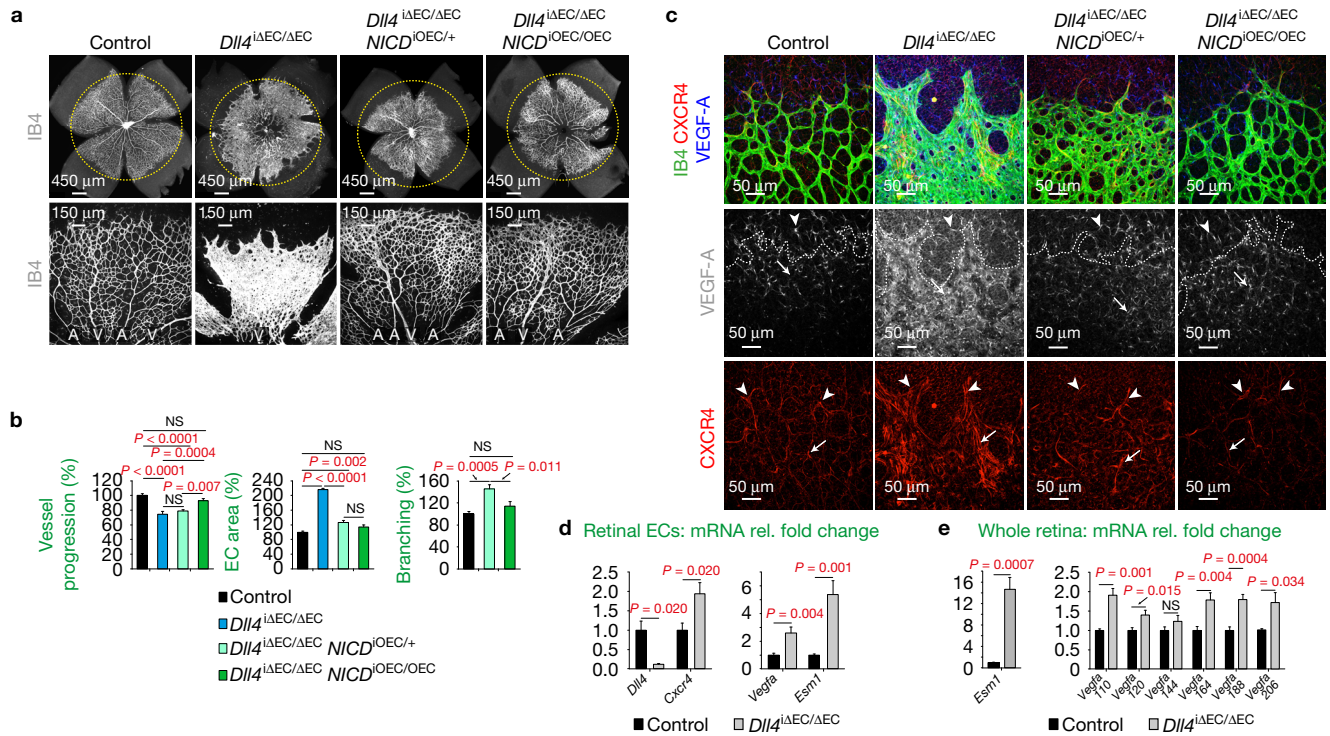


**Figure 1** Notch-dependent changes in endothelial CXCR4 and VEGF-A. (**a**) Representative overview (top panels) and high-magnification confocal images (bottom panels) of isolectin B4 (IB4)-stained P6 control, *Dll4*$^{i\Delta EC/\Delta EC}$, *Dll4*$^{i\Delta EC/\Delta EC}$ *NICD*$^{iOEC/+}$ and *Dll4*$^{i\Delta EC/\Delta EC}$ *NICD*$^{iOEC/OEC}$ retinas. Note hyperbranching and artery (A) and vein (V) formation defects in the *Dll4*$^{i\Delta EC/\Delta EC}$ vasculature, which were rescued in *Dll4*$^{i\Delta EC/\Delta EC}$ *NICD*$^{iOEC/OEC}$ double mutants. Circles indicate vessel outgrowth in the control. (**b**) Quantification of retinal vessel progression ($n=10$ control, 10 *Dll4*$^{i\Delta EC/\Delta EC}$, 9 *Dll4*$^{i\Delta EC/\Delta EC}$ *NICD*$^{iOEC/+}$ and 7 *Dll4*$^{i\Delta EC/\Delta EC}$ *NICD*$^{iOEC/OEC}$ retinas), EC area per field ($n=10$ control, 9 *Dll4*$^{i\Delta EC/\Delta EC}$, 10 *Dll4*$^{i\Delta EC/\Delta EC}$ *NICD*$^{iOEC/+}$ and 12 *Dll4*$^{i\Delta EC/\Delta EC}$ *NICD*$^{iOEC/OEC}$ retinas) and branching points ($n=10$ control, 10 *Dll4*$^{i\Delta EC/\Delta EC}$ *NICD*$^{iOEC/+}$ and 12 *Dll4*$^{i\Delta EC/\Delta EC}$ *NICD*$^{iOEC/OEC}$ retinas). Data represent mean ± s.e.m. *P* values, one-way ANOVA with Tukey's multiple comparison *post hoc* test. (**c**) Confocal images of IB4-stained (green), VEGF-A-stained (blue/white) and CXCR4-stained (red) P6 *Dll4*$^{i\Delta EC/\Delta EC}$, *Dll4*$^{i\Delta EC/\Delta EC}$ *NICD*$^{iOEC/+}$, *Dll4*$^{i\Delta EC/\Delta EC}$ *NICD*$^{iOEC/OEC}$ and control retinal vessels. *Dll4*$^{i\Delta EC/\Delta EC}$ mutants exhibit elevated VEGF-A in vascular plexus (arrows) and avascular tissue (arrowheads). Increased CXCR4 expression in IB4-positive *Dll4*$^{i\Delta EC/\Delta EC}$ sprouts (arrowheads) and plexus vessels (arrows) was reduced after expression of active Notch in *Dll4*$^{i\Delta EC/\Delta EC}$ mutant ECs. The dotted lines mark the leading edge of the vascular plexus. (**d**) Quantitative RT–PCR (RT–qPCR) analysis of *Dll4* ($n=5$ control and 8 *Dll4*$^{i\Delta EC/\Delta EC}$ mice), *Cxcr4* ($n=5$ control and 8 *Dll4*$^{i\Delta EC/\Delta EC}$ mice), *Vegfa* ($n=8$ control and 11 *Dll4*$^{i\Delta EC/\Delta EC}$ mice) and *Esm1* ($n=7$ control and 12 *Dll4*$^{i\Delta EC/\Delta EC}$ mice) transcripts in sorted *Dll4*$^{i\Delta EC/\Delta EC}$ and littermate control retinal ECs. Data represent mean ± s.e.m. *P* values, two-tailed unpaired *t*-test. (**e**) RT–qPCR analysis of *Esm1* and *Vegfa* splice variants in control and *Dll4*$^{i\Delta EC/\Delta EC}$ whole retina samples ($n=8$ control and 7 *Dll4*$^{i\Delta EC/\Delta EC}$ mice). Data represent mean ± s.e.m. *P* values, two-tailed unpaired *t*-test. NS, not significant.

restore Notch target gene expression in freshly isolated *Dll4*$^{i\Delta EC/\Delta EC}$ retinal ECs and rescued defects seen in the *Dll4*$^{i\Delta EC/\Delta EC}$ retinal vasculature (Fig. 1a,b and Supplementary Fig. 1c–g). The area covered by *Dll4*$^{i\Delta EC/\Delta EC}$ *NICD*$^{iOEC/+}$ or *Dll4*$^{i\Delta EC/\Delta EC}$ *NICD*$^{iOEC/OEC}$ vessels was reduced close to control levels and vascular outgrowth was restored. The number of branch points, uncountable in *Dll4*$^{i\Delta EC/\Delta EC}$ mutants, was normalized in *Dll4*$^{i\Delta EC/\Delta EC}$ *NICD*$^{iOEC/OEC}$ retinas, and arteries and veins were clearly detectable (Fig. 1a,b and Supplementary Fig. 1c).

To explain how downstream effectors might influence the NICD-dependent rescue of the *Dll4* loss-of-function phenotype, we investigated two known important regulators of EC behaviour, namely CXCR4 and endothelial VEGF-A. CXCR4, the receptor for the chemokine CXCL12, also known as SDF1, provides directional cues for growing blood and lymphatic vessels[21–25]. Consistent with published data on tip-cell-enriched genes[24], CXCR4 immunostaining decorated endothelial sprouts in P6 retinas (Fig. 1c). CXCR4 protein and *Cxcr4* mRNA levels were upregulated in the *Dll4*$^{i\Delta EC/\Delta EC}$ vasculature, whereas CXCR4 immunostaining was substantially reduced in *Dll4*$^{i\Delta EC/\Delta EC}$ *NICD*$^{iOEC/+}$ or *Dll4*$^{i\Delta EC/\Delta EC}$ *NICD*$^{iOEC/OEC}$ compound mutants (Fig. 1c,d). VEGF-A is expressed by hypoxic cells resulting in paracrine activation of ECs[26,27], but the growth factor is also produced by ECs to control survival and angiogenesis in a presumably autocrine fashion[28–30]. *Vegfa* transcripts were significantly increased in freshly isolated *Dll4*$^{i\Delta EC/\Delta EC}$ retinal ECs and strong VEGF-A immunostaining was seen within the hypertrophic mutant vessels (Fig. 1c–e and Supplementary Fig. 1d). Endothelial VEGF-A staining was no longer detectable after NICD-mediated rescue of the *Dll4*$^{i\Delta EC/\Delta EC}$ phenotype, which also reduced VEGF-A expression in the avascular retina (Fig. 1c and Supplementary Fig. 1d). VEGF-A immunosignals were, however, occasionally seen in dense endothelial foci of *Dll4*$^{i\Delta EC/\Delta EC}$ *NICD*$^{iOEC/OEC}$ compound mutants, which are likely to reflect small areas of insufficient rescue (Supplementary Fig. 1e). Indicating that the levels of endothelial Notch activation were not excessively high, transcript levels of the Notch target genes *Hes1*, *Hey1* and *Efnb2* were close to control in ECs from *NICD*$^{iOEC/OEC}$ homozygotes and, unexpectedly, elevated about twofold in *NICD*$^{iOEC/+}$ heterozygotes (Supplementary Fig. 1f).

Consistent with the observed regulation of endothelial VEGF-A by Notch, expression of ESM1, a tip cell marker and VEGF-regulated gene product[31,32], was upregulated in *Dll4*$^{i\Delta EC/\Delta EC}$ retinal vessels (Fig. 1d and Supplementary Fig. 1g). Upregulation of *Esm1* and specific *Vegfa* isoforms was also detectable in whole retina lysates (Fig. 1e). As for CXCR4, ESM1 immunostaining was strongly reduced after NICD-mediated rescue of *Dll4*$^{i\Delta EC/\Delta EC}$ mutants, which failed to fully restore the tip-cell-restricted pattern of ESM1 distribution (Supplementary Fig. 1g). Together, these data identify endothelial VEGF-A and CXCR4 as potential Notch-dependent regulators of angiogenesis. Overlapping CXCR4 and VEGF-A immunostaining in the angiogenic front suggests that the two pathways might be linked (Supplementary Fig. 2f).

### VEGF-A and CXCR4 in Notch-controlled angiogenesis

To address the role of endothelial VEGF-A, we generated EC-specific and inducible *Vegfa*$^{i\Delta EC/\Delta EC}$ mutants. Consistent with previous reports on endothelial VEGF-A expression[28–30], loss of a single or both *Vegfa* alleles in ECs led to substantially reduced vessel growth and branching (Fig. 2a,b and Supplementary Fig. 2a–c). Pharmacological inhibition of Notch by administration of the γ-secretase inhibitor DAPT led to increased EC density and sprouting in proximity of the avascular region expressing VEGF-A, but had little effect in the *Vegfa*$^{i\Delta EC/+}$ or *Vegfa*$^{i\Delta EC/\Delta EC}$ central retina (Fig. 2a–c and Supplementary Fig. 2a–c). Consistent with these regional differences, VEGF-A immunostaining was readily detectable in the avascular retinal tissue but not within the DAPT-treated *Vefga*$^{i\Delta EC/\Delta EC}$ vasculature (Fig. 2d). Likewise, increases in Dll4 and ESM1 immunostaining were pronounced in DAPT-treated controls but diminished in *Vefga*$^{i\Delta EC/\Delta EC}$ retinas (Fig. 2e and Supplementary Fig. 2e). These data argue that Notch-dependent regulation of endothelial VEGF-A plays a key role in the control of EC behaviour.

CXCR4 expression in the P6 wild-type retina was detected in tip cells, in some ECs of the vessel plexus, in arterial ECs and outside the vasculature, while the ligand CXCL12 was expressed by astrocytes in proximity of endothelial sprouts and by perivascular cells (Fig. 3a,b). Inducible and EC-specific inactivation of the *Cxcr4* gene led to reduced vessel outgrowth, density and branching, and impaired EC proliferation and sprouting in the P6 *Cxcr4*$^{i\Delta EC/\Delta EC}$ retinal vasculature (Fig. 3c,d and Supplementary Fig. 3a,b,e). A similar phenotype was obtained in *Cxcr4*$^{i\Delta EC/KO}$ mice carrying one constitutive and one conditional knockout allele (Fig. 3e and Supplementary Fig. 3a,c,f). Immunostaining of the tip cell marker ESM1 was unchanged in *Cxcr4* loss-of-function mutants despite increased VEGF-A expression in the avascular retina (Fig. 3f and Supplementary Fig. 3d). Analysis of freshly isolated *Cxcr4*$^{i\Delta EC/\Delta EC}$ retinal ECs showed no change in *Esm1* transcript expression, whereas *Vegfa* was slightly but not statistically significantly increased (Supplementary Fig. 3g). CXCR4 does not appear to act upstream of Notch, as transcripts for *Dll4*, *Jag1* and the Notch targets *Hey1* and *Hes1* were not significantly changed in isolated *Cxcr4*$^{i\Delta EC/\Delta EC}$ retinal ECs (Supplementary Fig. 3h).

Consistent with the upregulation of CXCR4 in *Dll4*$^{i\Delta EC/\Delta EC}$ retinal ECs (Fig. 1c,d), loss of the chemokine receptor led to reduced sprouting after Notch inhibition (Fig. 4a,b and Supplementary Fig. 4a,b) despite strong upregulation of VEGF-A at the vascular growth front (Fig. 3f). Acute pharmacological inhibition of CXCL12–CXCR4 signalling with AMD3100 led to significantly reduced sprouting and a blunt appearance of the distal *Dll4*$^{i\Delta EC/\Delta EC}$ vessel plexus (Fig. 4c,d and Supplementary Fig. 4c). Likewise, genetic approaches combining EC-specific mutant alleles of *Cxcr4* and *Rbpj*, the essential downstream mediator of Notch-induced gene transcription[33], led to significant reductions in vessel outgrowth, EC-covered area and sprouting relative to control littermates (Fig. 4e,f and Supplementary Fig. 4d,e). Impaired sprouting, visible as a blunt angiogenic growth front, was also seen in *Cxcr4*$^{i\Delta EC/\Delta EC}$ *Dll4*$^{i\Delta EC/\Delta EC}$ double mutants (Supplementary Fig. 4f,g).

### Investigation of Notch and VEGF-A-mediated processes

Next, we investigated whether Notch signalling and the transcription factor RBPJ directly regulate expression of *Cxcr4*, *Vegfa* and *Esm1* in ECs. Chromatin immunoprecipitation (ChIP) in the murine endothelial cell line MS1 showed strong RBPJ binding to the *Vegfa* locus and the positive control *Hes1*, whereas RBPJ occupancy to putative binding sites was weak for *Cxcr4* and absent for *Esm1* (Fig. 5a and Supplementary Fig. 5b). DAPT treatment downregulated expression of the Notch target genes *Hes1*, *Dll4* and *Nrarp* indicating active Notch signalling in MS1 cells (Supplementary Fig. 5c). Active histone modification, namely H3K27ac, H3K4me1, H3K4me3 and H3K9ac, but not the repressive marks H3K9me3 and H3K27me3, were enriched at the RBPJ-binding site in *Hes1* (Fig. 5b,c and Supplementary Fig. 5a,b). In contrast, *Cxcr4*, *Vegfa* and *Esm1* were only marginally altered by DAPT treatment in MS1 cells. Both active and repressive histone marks were found at RBPJ-bound sites of *Cxcr4*, *Vegfa* and *Esm1*, suggesting a poised state (Fig. 5b,c and Supplementary Fig. 5a–c). These data are consistent with a potential direct negative regulation of *Vegfa* expression by RBPJ in ECs similar to what has been previously described for adult cardiomyocytes[34]. Accordingly, VEGF-A immunosignals were strongly upregulated in *Rbpj*$^{i\Delta EC/\Delta EC}$ retinal ECs *in vivo* (Supplementary Fig. 5d).

Outside the endothelium, VEGF-A was upregulated in the peripheral avascular tissue in *Cxcr4*$^{i\Delta EC/KO}$ (Fig. 3f) and *Dll4*$^{i\Delta EC/\Delta EC}$ (Fig. 1c,d) retinas as well as in *NICD*$^{iOEC/OEC}$ samples (Supplementary Fig. 5g,h,n). Isolated *NICD*$^{iOEC/OEC}$ retinal ECs showed significantly increased transcript levels for *Dll4*, a known Notch target gene, but also for *Vegfa* and *Esm1* (Supplementary Fig. 5e). Endothelial *Cxcr4* transcripts were also increased, which was, however, not reflected in immunostainings (Fig. 5d and Supplementary Fig. 5e,i). Next, we investigated the contribution of VEGF-A/VEGFR2 in the regulation of CXCR4 and ESM1. Notch activation has been linked to reduced VEGFR2 expression[6,35–38]. Our previous work argued that Notch inhibition triggers retinal angiogenesis after genetic or pharmacological interference with VEGFR2 (ref. 8), while another study attributed such effects to residual VEGFR2 activity[5]. A stringent genetic strategy combining conditional and constitutive knockout alleles of murine *Flk1* led to highly diminished expression of VEGFR2, which strongly impaired vascular growth in the resulting *Flk1*$^{i\Delta EC/KO}$ mutants (Fig. 5e and Supplementary Fig. 5j). This was accompanied by strong upregulation of VEGF-A immunostaining and *Vegfa* transcripts but reduced expression of ESM1, Dll4 and CXCR4 at the angiogenic front (Fig. 5f,g and Supplementary Fig. 5f,j,k). Global levels of *Cxcr4* and *Dll4* transcripts were slightly but significantly reduced in freshly sorted *Flk1*$^{i\Delta EC/KO}$ retinal ECs (Supplementary Fig. 5f). Consistent with the role of VEGF-A/VEGFR2 interactions as a survival signal, EC death was profoundly increased in the *Flk1*$^{i\Delta EC/KO}$ vasculature (Supplementary Fig. 5l).

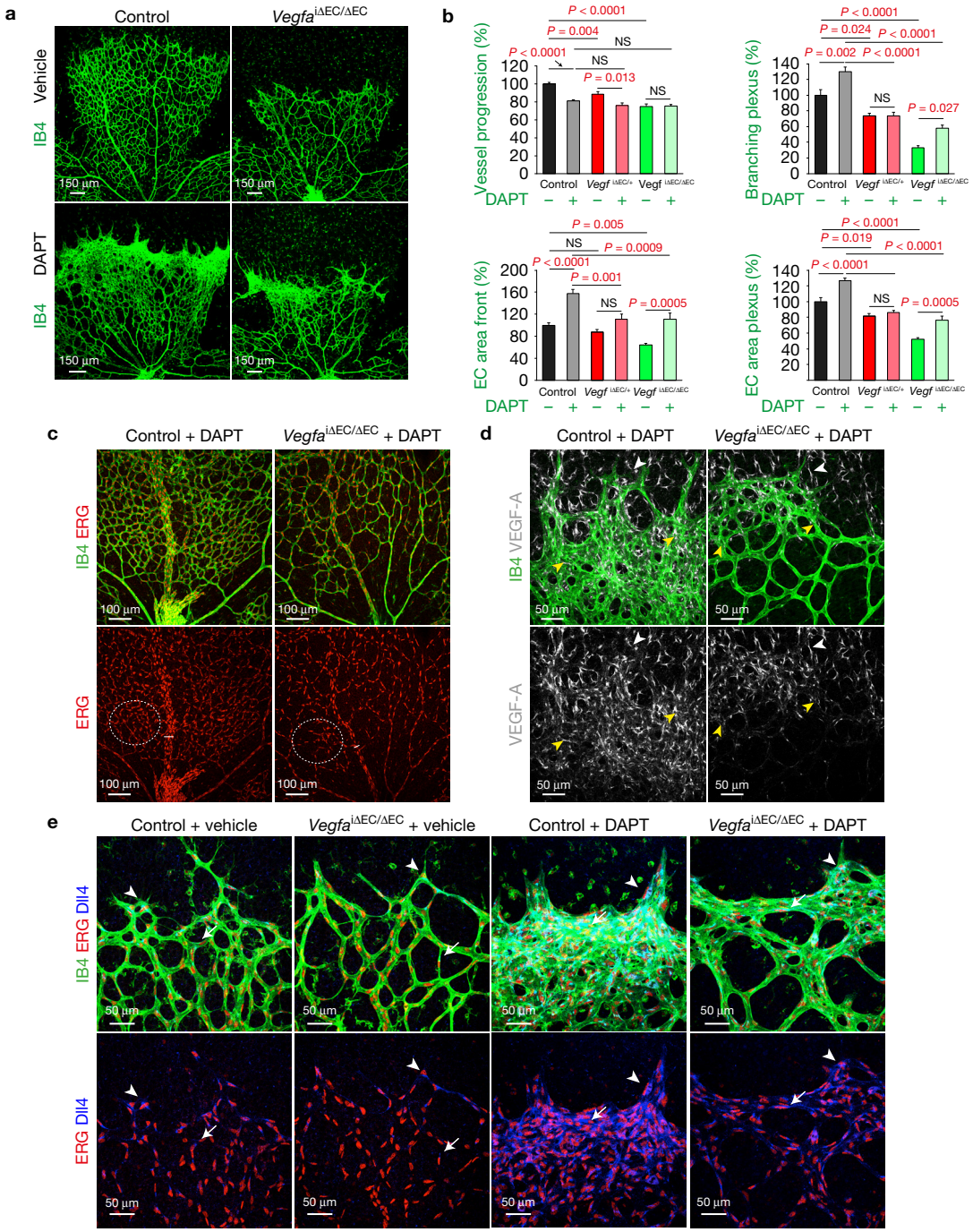


**Figure 2** Role of endothelial VEGF-A in Notch-controlled angiogenesis. (**a**) Representative confocal images showing IB4-stained *Vegfa*$^{i\Delta EC/\Delta EC}$ and control P6 retinal vessels after treatment with vehicle or DAPT (36 h). Note the reduced angiogenic response to DAPT in the *Vegfa*$^{i\Delta EC/\Delta EC}$ plexus, whereas the response at the front was more similar to the DAPT-treated control. (**b**) Quantitative analysis of vascular parameters of vehicle- or DAPT-treated control, *Vegfa*$^{i\Delta EC/+}$ and *Vegfa*$^{i\Delta EC/\Delta EC}$ mice: retinal vessel progression ($n=11$ vehicle- and 6 DAPT-treated control retinas, $n=10$ vehicle- and 5 DAPT-treated *Vegfa*$^{i\Delta EC/+}$ retinas and $n=7$ vehicle- and 9 DAPT-treated *Vegfa*$^{i\Delta EC/\Delta EC}$ retinas), EC area in the front region ($n=8$ vehicle- and 5 DAPT-treated control retinas, $n=6$ vehicle- and 5 DAPT-treated *Vegfa*$^{i\Delta EC/+}$ and $n=6$ vehicle- and 6 DAPT-treated *Vegfa*$^{i\Delta EC/\Delta EC}$), EC area in the central plexus and branching points ($n=5$ vehicle- and 8 DAPT-treated control retinas, $n=5$ vehicle- and 7 DAPT-treated *Vegfa*$^{i\Delta EC/+}$ retinas and $n=6$ vehicle- and 5 DAPT-treated *Vegfa*$^{i\Delta EC/\Delta EC}$ retinas). Note significant changes also in heterozygous mutants. Data represent mean ± s.e.m. *P* values, two-way ANOVA with Tukey's multiple comparison *post hoc* test. NS, not significant. (**c**) Confocal images showing the central vessel plexus of DAPT-injected *Vegfa*$^{i\Delta EC/\Delta EC}$ and littermate control P6 retinas stained for IB4 (green) and ERG (EC nuclei, red). The white lines in the bottom panels indicate vein width; the encircled areas highlight differences in EC nuclei. (**d**) Confocal images of VEGF-A (white) and IB4 (green) whole-mount retina immunofluorescence for DAPT-treated *Vegfa*$^{i\Delta EC/\Delta EC}$ and control P6 mice. Reduced VEGF-A (yellow arrowheads) signal in retinal vessels of DAPT-injected *Vegfa*$^{i\Delta EC/\Delta EC}$ mutant relative to DAPT-treated control littermate. Note the comparable VEGF-A staining in the avascular retina (white arrowheads). (**e**) Confocal images of Dll4-stained (blue), ERG-stained (red) and IB4-stained (green) retinas of vehicle- or DAPT-treated control and *Vegfa*$^{i\Delta EC/\Delta EC}$ P6 mice. Dll4 was upregulated in sprouts (arrowheads) and the plexus region (arrows) of DAPT-treated control retinas. Note the reduced Dll4 upregulation in the *Vegfa*$^{i\Delta EC/\Delta EC}$ mutants.

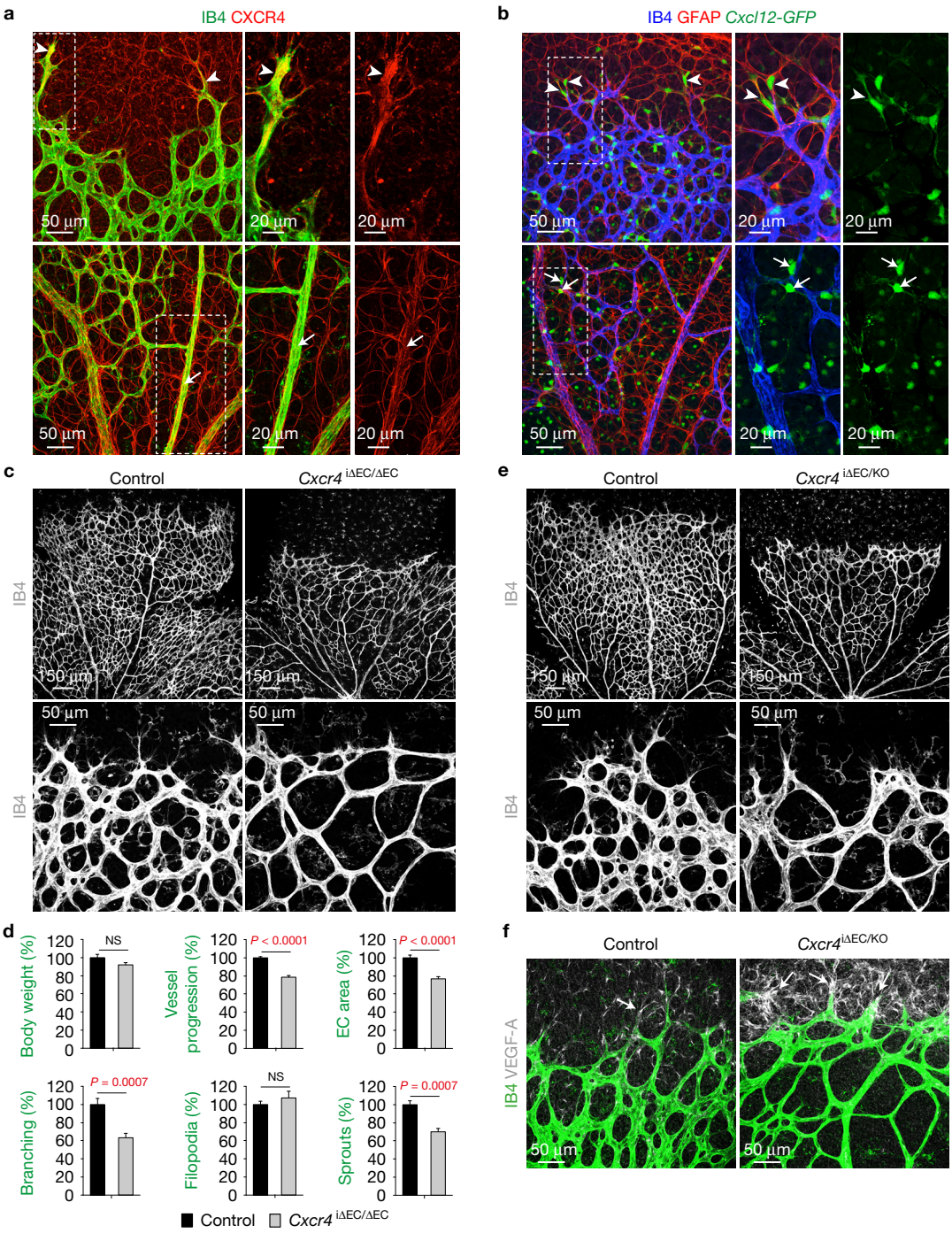


**Figure 3** Control of retinal angiogenesis by endothelial CXCR4. (**a**) Representative confocal images of CXCR4-stained (red) and IB4-stained (green) wild-type retinas. The panels in the centre and on the right show high magnifications of the outlined areas. CXCR4 expression labels ECs in sprouts (arrowheads) and arteries (arrows). CXCR4 signal was also detected in perivascular cells and astrocytes. (**b**) Nuclear GFP (green) expression in *Cxcl12-GFP* knock-in mice labels glial fibrillary acidic protein (GFAP)-positive (red) astrocytes (arrowheads) in direct proximity of IB4-stained (blue) sprouting ECs (top panels). GFP signal was also seen in vessel-associated cells (arrows) and outside the vasculature (bottom panels). (**c**) Representative overview and high-magnification confocal images showing IB4-stained control and $Cxcr4^{i\Delta EC/\Delta EC}$ retinal vessels. Note the reduced sprouting and branching at the vascular front of the mutant retinal vasculature. (**d**) Quantitative analysis of body weight ($n = 13$ control and 13 $Cxcr4^{i\Delta EC/\Delta EC}$ mice) and vascular parameters for $Cxcr4^{i\Delta EC/\Delta EC}$ and control littermates: retinal vessel progression ($n = 6$ control and 6 $Cxcr4^{i\Delta EC/\Delta EC}$ retinas), EC area ($n = 8$ control and 8 $Cxcr4^{i\Delta EC/\Delta EC}$ retinas), branching points ($n = 8$ control and 8 $Cxcr4^{i\Delta EC/\Delta EC}$ retinas), filopodia ($n = 6$ control and 6 $Cxcr4^{i\Delta EC/\Delta EC}$ retinas) and sprouts ($n = 6$ control and 6 $Cxcr4^{i\Delta EC/\Delta EC}$ retinas). Note the significant decrease in $Cxcr4^{i\Delta EC/\Delta EC}$ sprouts, branching points and EC area but no significant change in filopodia. Data represent mean ± s.e.m. *P* values, two-tailed unpaired *t*-test. NS, not significant. Quantifications of vessel progression, filopodia and sprouts are derived from two independent tamoxifen injections. (**e**) Representative overview and high-magnification confocal images of IB4-stained control and $Cxcr4^{i\Delta EC/KO}$ retinas. (**f**) Representative images of VEGF-A-stained (white) and IB4-stained (green) $Cxcr4^{i\Delta EC/KO}$ and control retinas. Note the increased VEGF-A immunosignal in the mutant avascular area (arrows).

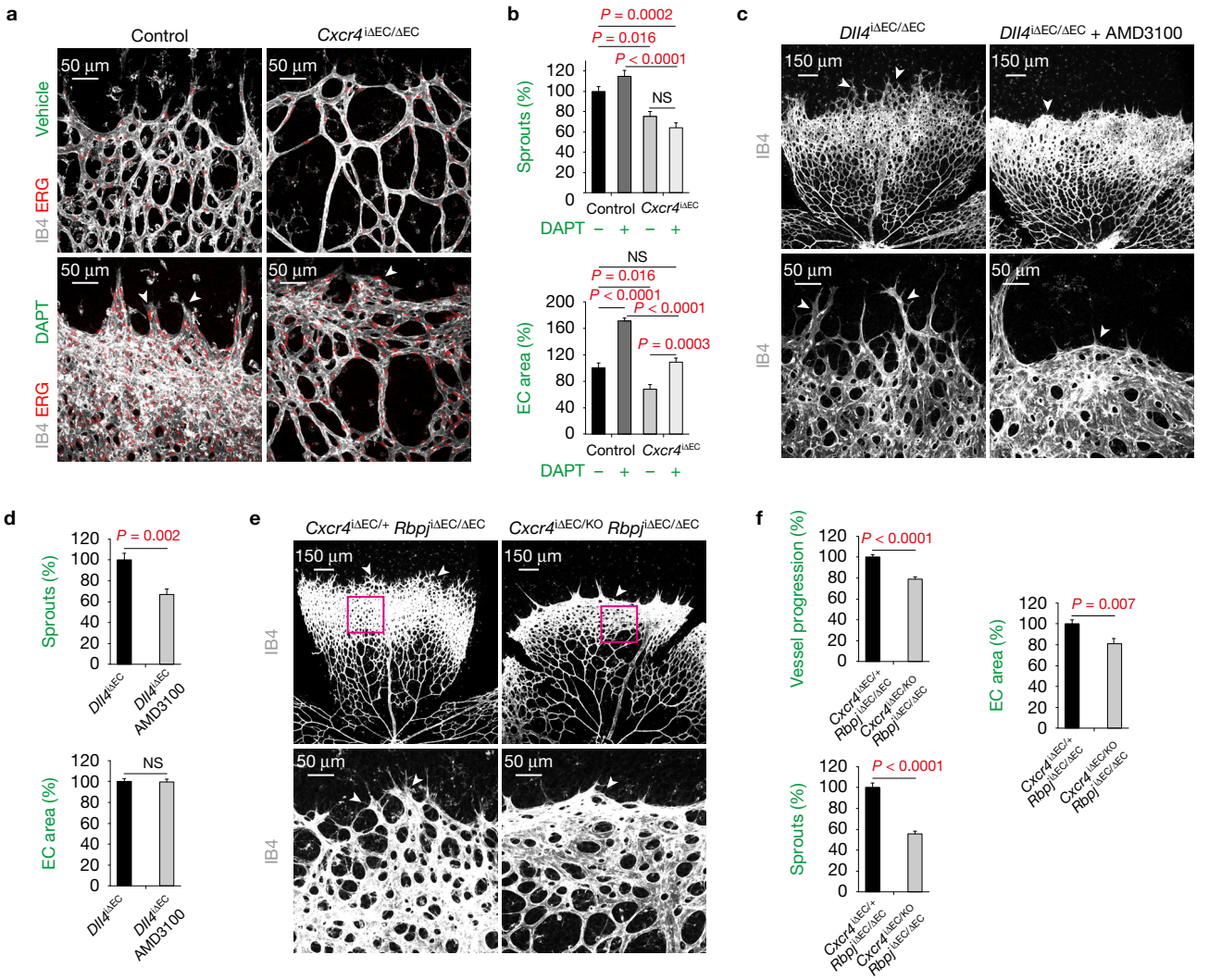


**Figure 4** CXCR4 is required for Notch-controlled endothelial sprouting. (**a**) Angiogenic response in *Cxcr4*$^{i\Delta EC/\Delta EC}$ and littermate control retinal vasculature (IB4) after treatment with vehicle or DAPT. Note the reduced sprouting (arrowheads) in the DAPT-treated *Cxcr4*$^{i\Delta EC/\Delta EC}$ retina. Endothelial nuclei are immunostained for ERG (red). (**b**) Quantitative analysis of sprouts ($n=6$ vehicle- and 5 DAPT-treated control retinas and $n=5$ vehicle- and 8 DAPT-treated *Cxcr4*$^{i\Delta EC/\Delta EC}$ retinas) and EC area ($n=7$ vehicle- and 7 DAPT-treated control retinas and $n=5$ vehicle- and 8 DAPT-treated *Cxcr4*$^{i\Delta EC/\Delta EC}$ retinas) in vehicle- or DAPT-treated *Cxcr4*$^{i\Delta EC/\Delta EC}$ or control retinas, as shown in **a**. Data represent mean ± s.e.m. *P* values, two-way ANOVA with Tukey's multiple comparison *post hoc* test. (**c**) Inhibition of CXCR4 with AMD3100 (24 h) led to reduced sprouting (arrowheads) in the *Dll4*$^{i\Delta EC/\Delta EC}$ retinal vasculature (note blunt vessel front in panels on the right). (**d**) Quantification of sprouts and EC area ($n=6$ untreated and 7 AMD3100-treated *Dll4*$^{i\Delta EC/\Delta EC}$ retinas) in the untreated or AMD3100-treated *Dll4* $^{i\Delta EC/\Delta EC}$ retinal vasculature, as shown in **c**. Note the reduction in sprout number but not EC area in the AMD3100-treated *Dll4*$^{i\Delta EC/\Delta EC}$ mutants. Data represent mean ± s.e.m. *P* values, two-tailed unpaired *t*-test. (**e**) Confocal images showing sprouting (arrowheads) defects in IB4-stained retinal vessels in *Cxcr4*$^{i\Delta EC/KO}$ *Rbpj*$^{i\Delta EC/\Delta EC}$ double homozygotes relative to the *Cxcr4*$^{i\Delta EC/+}$ *Rbpj*$^{i\Delta EC/\Delta EC}$ control. (**f**) Vascular parameters in *Cxcr4*$^{i\Delta EC/KO}$ *Rbpj*$^{i\Delta EC/\Delta EC}$ and *Cxcr4*$^{i\Delta EC/+}$ *Rbpj*$^{i\Delta EC/\Delta EC}$ controls: retinal vessel progression ($n=8$ *Cxcr4*$^{i\Delta EC/+}$ *Rbpj*$^{i\Delta EC/\Delta EC}$ and 8 *Cxcr4*$^{i\Delta EC/KO}$ *Rbpj*$^{i\Delta EC/\Delta EC}$ retinas), EC area ($n=8$ *Cxcr4*$^{i\Delta EC/+}$ *Rbpj*$^{i\Delta EC/\Delta EC}$ and 8 *Cxcr4*$^{i\Delta EC/KO}$ *Rbpj*$^{i\Delta EC/\Delta EC}$ retinas) and sprouts ($n=7$ *Cxcr4*$^{i\Delta EC/+}$ *Rbpj*$^{i\Delta EC/\Delta EC}$ and 7 *Cxcr4*$^{i\Delta EC/KO}$ *Rbpj*$^{i\Delta EC/\Delta EC}$ retinas). Fields demarcated by purple squares in **e** were used for EC area quantification. Data represent mean ± s.e.m. *P* values, two-tailed unpaired *t*-test. NS, not significant.

Despite the strong reduction in *Flk1*$^{i\Delta EC/KO}$ retinal vessels, DAPT treatment led to focal EC proliferation both inside and at the peripheral edge of the vascular plexus (Fig. 5e). These foci were positive for VEGF-A immunostaining (Fig. 5f) and might represent areas of residual signalling activity. ESM1 and CXCR4 were no longer upregulated in the DAPT-treated *Flk1*$^{i\Delta EC/KO}$ retinal endothelium (Fig. 5g and Supplementary Fig. 5m). Furthermore, treatment with anti-VEGF-A blocking antibodies suppressed ESM1 and CXCR4 upregulation in *NICD*$^{iOEC/OEC}$ retinal ECs (Fig. 5d). These data argue that enhanced EC proliferation and sprouting after Notch inhibition involve the upregulation of endothelial VEGF-A together with a VEGF-A/VEGFR2-dependent increase in CXCR4.

## Genetic analysis of tip cell behaviour

While genetic experiments affecting all ECs have provided valuable insights into the regulation of angiogenesis, it remains difficult to assign phenotypic alterations specifically to tip cells, stalk cells or other ECs *in vivo*. Such limitations can be overcome by generating mosaic

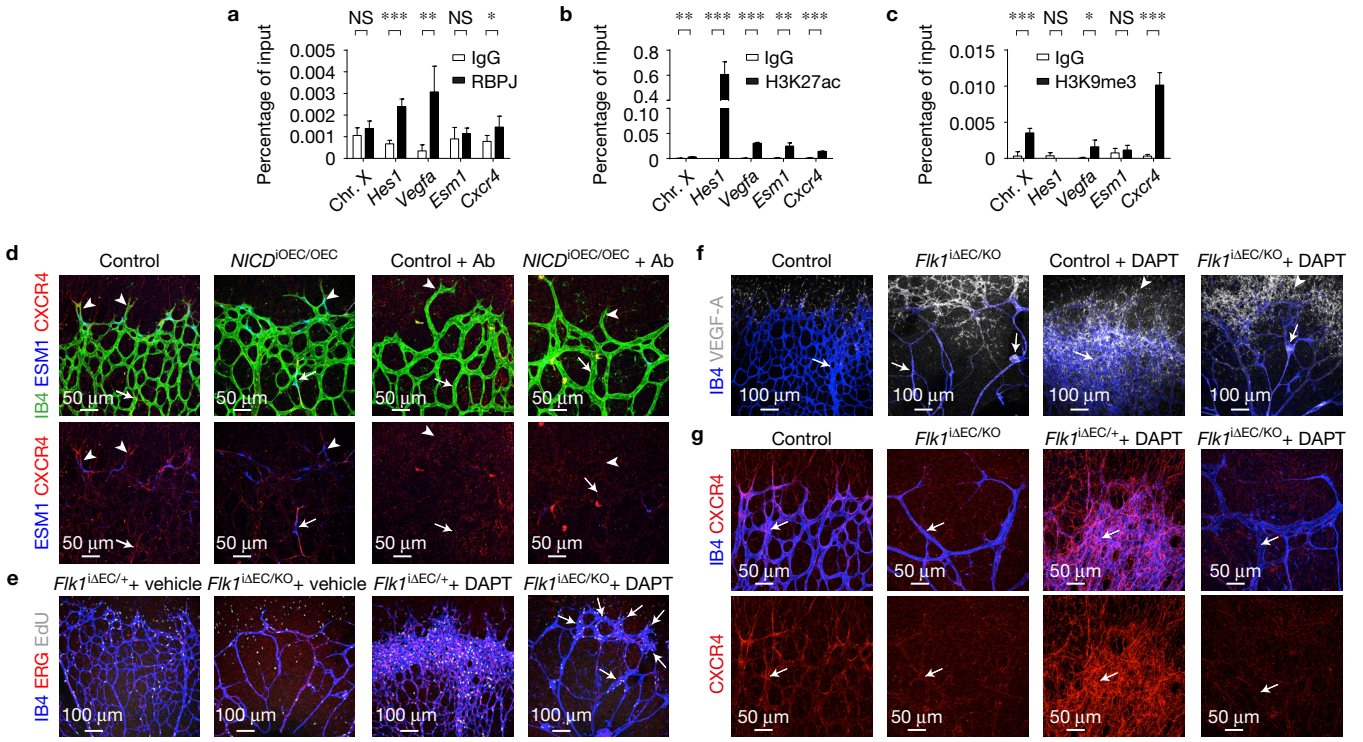


**Figure 5** Control of Notch- and VEGF-A-mediated-processes *in vitro* and *in vivo*. (**a**–**c**) ChIP analysis of RBPJ occupancy (**a**) and H3K27ac (**b**) and H3K9me3 (**c**) enrichment at the *Hes1*, *Vegfa*, *Esm1* and *Cxcr4* loci in mouse MS1 cells. A region located on chromosome X (Chr. X) was used as a control. Shown is the mean ± s.d. of 5 independent experiments in the case of RBPJ, 3 independent experiments in the case of H3K27ac and 2 independent experiments, measured twice each, in the case of H3K9me3 (NS, not significant; $^{*}P < 0.05$, $^{**}P < 0.01$, $^{***}P < 0.001$, two-tailed unpaired *t*-test). Statistics source data are provided in Supplementary Table 3. (**d**) Confocal images showing ESM1 (blue) and CXCR4 (red) immunostaining of retinal vasculature (IB4, green) in *NICD*$^{iOEC/OEC}$ and control mice injected with PBS or anti-VEGF-A antibody. The arrowheads indicate staining of tip cells, whereas the arrows indicate signal or absence of signal in the plexus. Note the appearance of IB4$^{+}$/CXCR4$^{+}$ cells outside the vasculature following antibody treatment. (**e**) Confocal images of *Flk1*$^{i\Delta EC/KO}$ and control (*Flk1*$^{i\Delta EC/+}$) retinas treated with vehicle or DAPT, as indicated. Mice were pulse-labelled with EdU (white) for 2 h before analysis and retinas were stained for IB4 (blue) and ERG (red), as indicated. Note the DAPT-induced EC proliferation (arrows) in the *Flk1*$^{i\Delta EC/KO}$ mutant. (**f**) Confocal images of VEGF-A-stained (white) and IB4-stained (blue) retinas from vehicle- or DAPT-treated *Flk1*$^{i\Delta EC/KO}$ and control P6 mice. Note the upregulation of VEGF-A in *Flk1*$^{i\Delta EC/KO}$ vessels (arrows) and avascular retina (arrowheads). Following DAPT treatment, VEGF-A was strongly upregulated in the control vasculature but labelled few EC foci in *Flk1*$^{i\Delta EC/KO}$ mutant vessels (arrows). Mice treated with vehicle are not littermates of those treated with DAPT. (**g**) Representative images of CXCR4-stained (red) and IB4-stained (blue) *Flk1*$^{i\Delta EC/KO}$ and control retinal vessels from mice injected with vehicle or DAPT. Note the strongly reduced CXCR4 immunosignal in the *Flk1*$^{i\Delta EC/KO}$ ECs (arrowheads and arrows). DAPT induced CXCR4 upregulation in the control (*Flk1*$^{i\Delta EC/+}$) but not in the *Flk1*$^{i\Delta EC/KO}$ plexus (arrows). Mice treated with vehicle are not littermates of those treated with DAPT.

mutants or Cre transgenic strains targeting EC subsets[39,40]. Here, we made use of *Esm1-CreERT2* transgenic mice[32], which mimic the tip-cell-specific expression of ESM1 in retina[31], in combination with the *R26-mTmG*$^{T/+}$ Cre reporter[41] (Fig. 6a,b and Supplementary Fig. 6a). Following injection with a low dose of 4-hydroxytamoxifen (4-OHT), *Esm1-CreERT2* transgenics enable irreversible genetic labelling and fate mapping of tip cells[42] (Fig. 6a,b). Analysis of retinas from P6 mice, which had received a single 4-OHT pulse at different time points prior to analysis, indicated that *Esm1-CreERT2*-labelled (GFP$^{+}$) ECs expand over time and populate the angiogenic growth front even after a 96 h chase period (Fig. 6b). Similar experiments with the multicolour Cre reporter *R26R-Confetti*[43] established that this expansion of *Esm1-CreERT2*-labelled ECs is clonal (Fig. 6c and Supplementary Fig. 6b). As we have previously reported[42], an increasing number of *Esm1-CreERT2*-labelled ECs was found inside the arterial but not venous endothelium (Fig. 6b).

Next, we used the *Esm1-CreERT2* strain to investigate CXCR4 function in tip cells. *Cxcr4*$^{i\Delta TC/KO}$ mice were generated by combining a global knockout and a conditional, tip cell-specific mutant *Cxcr4* allele in the *R26-mTmG* Cre reporter background. Compared with GFP$^{+}$ cells in *Cxcr4*$^{+/KO}$ littermate controls, the overall number of labelled *Cxcr4*$^{i\Delta TC/KO}$ ECs was not reduced, but mutant cells were significantly less abundant in vessel sprouts (Fig. 6d and Supplementary Fig. 6c,d). Those GFP$^{+}$ *Cxcr4*$^{i\Delta TC/KO}$ cells located in sprouts were frequently excluded from the leading position, which was instead occupied by unrecombined (GFP$^{-}$) ECs (Fig. 6d). Thus, loss of CXCR4 impairs the ability of retinal ECs to act as tip cells.

## Regulation of retinal tip cell behaviour by the Notch pathway

Dll4 is a frequently used tip cell marker and is thought to suppress tip-like behaviour in adjacent stalk cells by activating Notch[4,6,9,44]. We used *Esm1-CreERT2*-mediated inactivation of *Notch1* in combination with the *R26-mTmG* Cre reporter to track the resulting GFP$^{+}$ *Notch1*$^{i\Delta TC/\Delta TC}$ ECs in the retina. Consistent with the suppression of EC proliferation by Notch, *Notch1*$^{i\Delta TC/\Delta TC}$ ECs were enriched and ESM1 expression was enhanced in GFP$^{+}$ cells at the P6 retinal

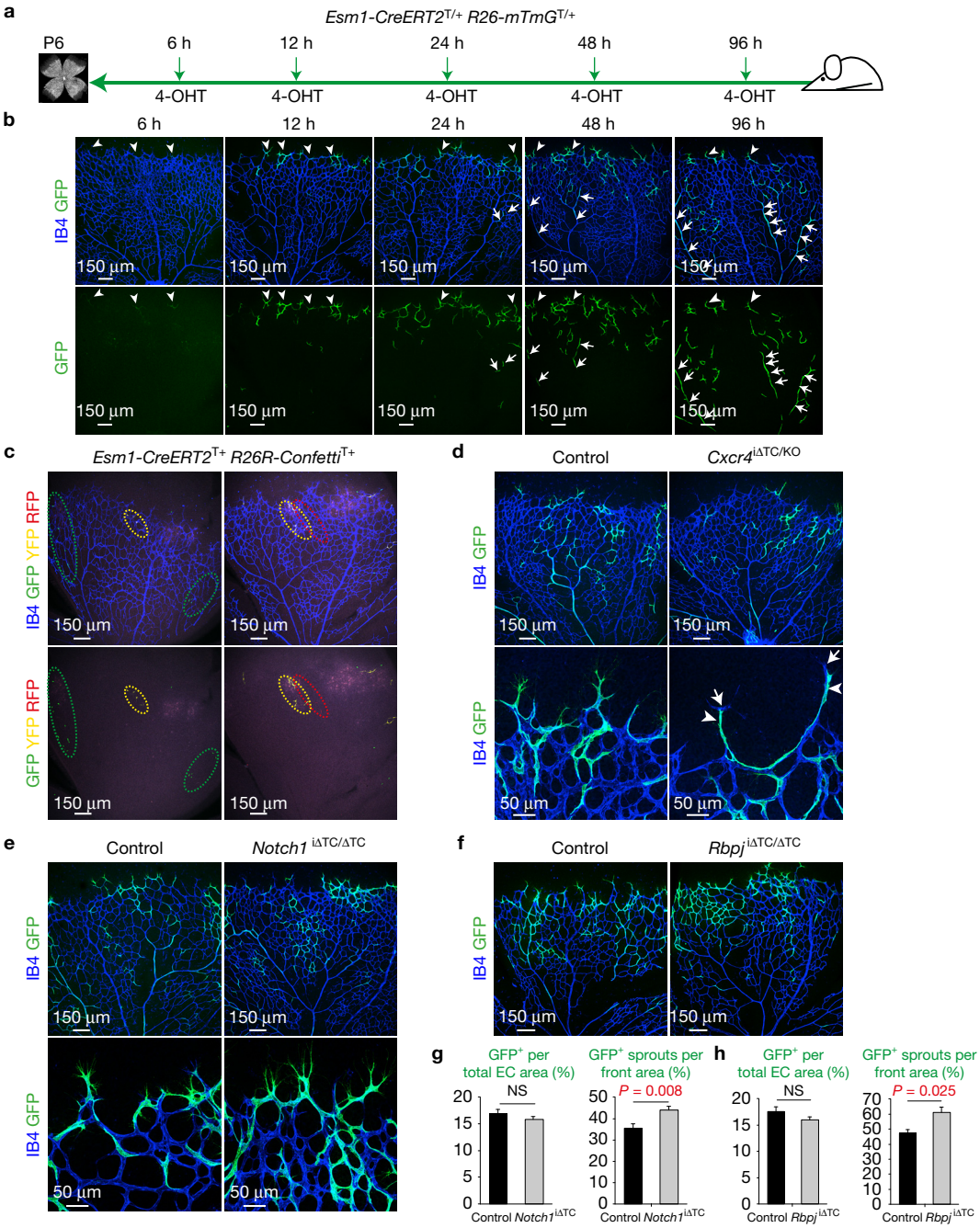


**Figure 6** Genetic tracking and manipulation of tip cells *in vivo*. (**a**) Scheme of the time course of 4-hydroxytamoxifen (4-OHT) administration and lineage tracing in *Esm1-CreERT2*$^{T/+}$ *R26-mTmG*$^{T/+}$ mutant mice. (**b**) Tracking of GFP-expressing (green) ECs in the *Esm1-CreERT2*$^{T/+}$ *R26-mTmG*$^{T/+}$ retinal vasculature (IB4, blue). GFP expression appeared at 6 h after 4-OHT injection in some tip cells and labelled sprouts up to 96 h after injection (arrowheads). While some recombined cells appeared in arteries after 24 h, substantially more GFP$^+$ ECs were incorporated at 48 and 96 h (arrows). (**c**) Clonal expansion (encircled areas) of *Esm1-CreERT2*$^{T/+}$ *R26R-Confetti*$^{T/+}$ tip-derived ECs in arteries or at the angiogenic front. IB4 labels ECs (blue), while nuclear GFP, cytoplasmic RFP and YFP mark the recombined cells. (**d**) Overview and high-magnification confocal images of IB4 (blue) and GFP (green) staining in *Cxcr4*$^{i\Delta TC/KO}$ (*Esm1-CreERT2*$^{T/+}$ *Cxcr4*$^{lox/KO}$ *R26-mTmG*$^{T/+}$) and control (*Esm1-CreERT2*$^{T/+}$ *Cxcr4*$^{+/KO}$ *R26-mTmG*$^{T/+}$) retinas at 96 h after 4-OHT injection. GFP$^+$ *Cxcr4*$^{i\Delta TC/KO}$ ECs (arrowheads) in sprouts were excluded from the most distal position (arrows). (**e**) Representative overview and high-magnification confocal images of IB4-stained (blue) vasculature and GFP-labelled (green) *Notch1*$^{i\Delta TC/\Delta TC}$ (*Esm1-CreERT2*$^{T/+}$ *Notch1*$^{lox/lox}$ *R26-mTmG*$^{T/+}$) and control (*Esm1-CreERT2*$^{T/+}$ *R26-mTmG*$^{T/+}$) retinas at 96 h after 4-OHT injection. (**f**) IB4 (blue) and GFP (green) staining of *Rbpj*$^{i\Delta TC/\Delta TC}$ (*Esm1-CreERT2*$^{T/+}$ *Rbpj*$^{lox/lox}$ *R26-mTmG*$^{T/+}$) and control (*Esm1-CreERT2*$^{T/+}$ *Rbpj*$^{lox/+}$ *R26-mTmG*$^{T/+}$) retinas at 72 h after 4-OHT injection. (**g**) Quantitative analysis of *Notch1*$^{i\Delta TC/\Delta TC}$ and control recombined GFP$^+$ cells per total endothelial area ($n=8$ control and 10 *Notch1*$^{i\Delta TC/\Delta TC}$ retinas) and of recombined GFP$^+$ sprouts per front area ($n=8$ control and 10 *Notch1*$^{i\Delta TC/\Delta TC}$ retinas) at 96 h after 4-OHT injection. Data represent mean ± s.e.m. *P* values, two-tailed unpaired *t*-test. (**h**) Quantitative analysis of *Rbpj*$^{i\Delta TC/\Delta TC}$ and control recombined GFP$^+$ cells per total endothelial area ($n=7$ *Rbpj*$^{i\Delta TC/+}$ control and 6 *Rbpj*$^{i\Delta TC/\Delta TC}$ retinas) and of recombined GFP$^+$ sprouts per front area ($n=7$ *Rbpj*$^{i\Delta TC/+}$ control and 6 *Rbpj*$^{i\Delta TC/\Delta TC}$ retinas) at 72 h after 4-OHT injection. Data represent mean ± s.e.m. *P* values, two-tailed unpaired *t*-test. NS, not significant.

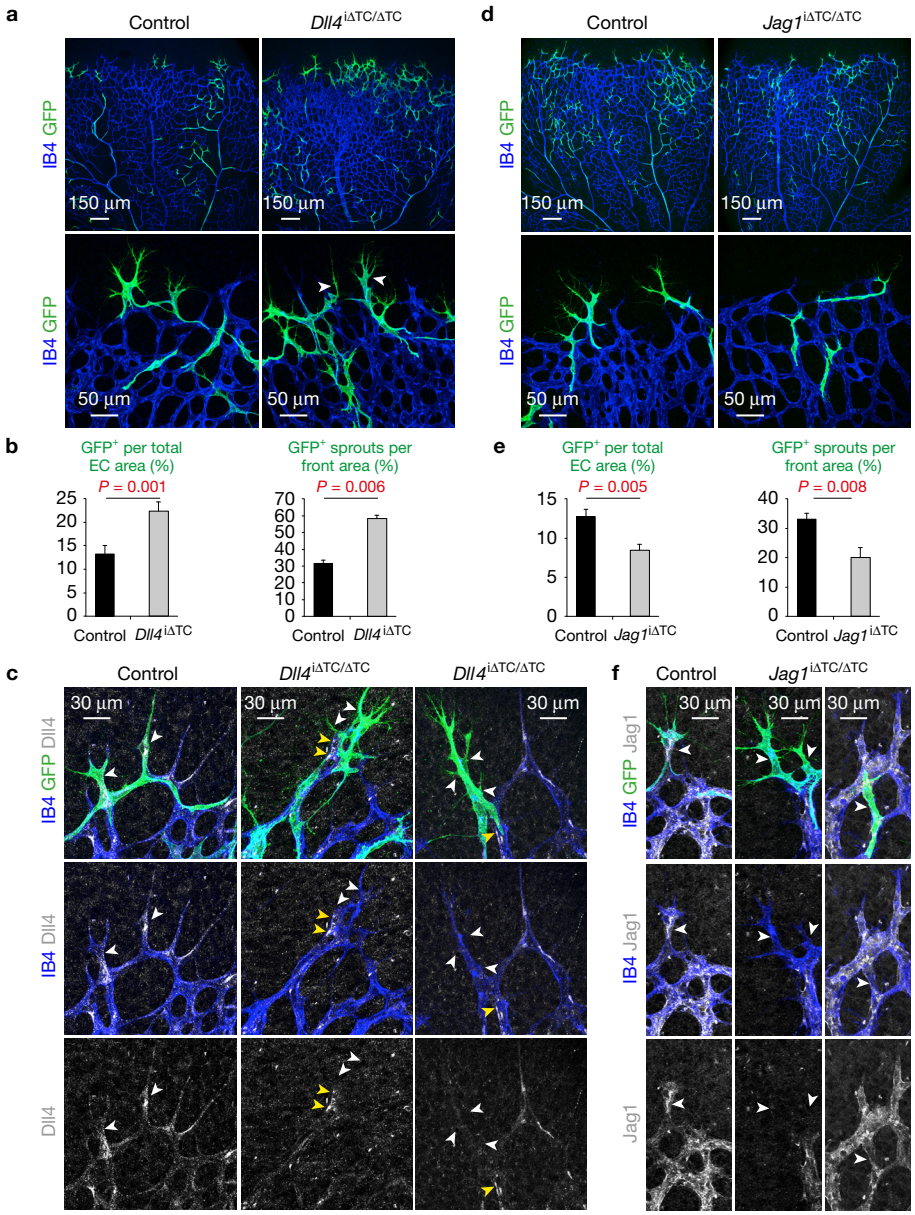


**Figure 7** Control of tip cell behaviour by Dll4 and Jag1. (**a**) Representative overview and high-magnification confocal images of GFP-labelled (green) *Dll4*$^{iΔTC/ΔTC}$ (*Esm1-CreERT2*$^{T/+}$ *Dll4*$^{lox/lox}$ *R26-mTmG*$^{T/+}$) and control (*Esm1-CreERT2*$^{T/+}$ *R26-mTmG*$^{T/+}$) ECs in the retinal vasculature (IB4, blue) at 96 h after 4-OHT administration. The arrowheads indicate Dll4-deficient GFP$^{+}$ tips displaying increased extension of protrusions and filopodia. (**b**) Quantitative analysis of recombined GFP$^{+}$ cells per total endothelial area ($n=7$ control and 8 *Dll4*$^{iΔTC/ΔTC}$ retinas) and of recombined GFP$^{+}$ sprouts per front area ($n=7$ control and 8 *Dll4*$^{iΔTC/ΔTC}$ retinas) at 96 h after 4-OHT injection. Note the significantly increased number of *Dll4*$^{iΔTC/ΔTC}$ ECs in sprouts and total EC area. Data represent mean ± s.e.m. *P* values, two-tailed unpaired *t*-test. (**c**) Confocal images of IB4 (blue), GFP (green) and Dll4 (white) staining in P6 *Dll4*$^{iΔTC/ΔTC}$ and control retinas at 48 h after 4-OHT injection. Note the Dll4 immunosignal in recombined control but not *Dll4*$^{iΔTC/ΔTC}$ tip cells (white arrowheads). The yellow arrowheads indicate Dll4 immunosignal in unrecombined stalk cells in direct proximity of Dll4-deficient tips. Images are representative of three mice analysed. (**d**) Maximum intensity projections of GFP-labelled (green) *Jag1*$^{iΔTC/ΔTC}$ (*Esm1-CreERT2*$^{T/+}$ *Jag1*$^{lox/lox}$ *R26-mTmG*$^{T/+}$) and control (*Esm1-CreERT2*$^{T/+}$ *R26-mTmG*$^{T/+}$) ECs in the retinal vasculature (IB4, blue) at 96 h after 4-OHT administration. The *Jag1*$^{iΔTC/ΔTC}$ cells showed no overt morphological changes. Note the reduction in Jag1-deficient GFP$^{+}$ tip cells. (**e**) Quantitative analysis of recombined GFP$^{+}$ cells per total endothelial area ($n=7$ control and 6 *Jag1*$^{iΔTC/ΔTC}$ retinas) and of recombined GFP$^{+}$ sprouts per front area ($n=7$ control and 6 *Jag1*$^{iΔTC/ΔTC}$ retinas) at 96 h after 4-OHT injection. *Jag1*$^{iΔTC/ΔTC}$ ECs were less abundant throughout the vasculature and in sprouts. Data represent mean ± s.e.m. *P* values, two-tailed unpaired *t*-test. (**f**) IB4 (blue), GFP (green) and Jag1 (white) staining of *Jag1*$^{iΔTC/ΔTC}$ and control retinas at 96 h after 4-OHT injection. Note the Jag1 immunostaining in ECs at the control angiogenic front but lost or reduced signal in GFP$^{+}$ *Jag1*$^{iΔTC/ΔTC}$ ECs (arrowheads).

angiogenic front after a single 4-OHT injection at 96 h prior to analysis (Fig. 6e,g and Supplementary Fig. 6e). A similar approach for the analysis of *Rbpj*$^{iΔTC/ΔTC}$ ECs (see Methods) also led to enrichment of GFP-labelled mutant cells at the angiogenic front (Fig. 6f,h). No significant change was seen in the abundance of *Notch1*$^{iΔTC/ΔTC}$ or *Rbpj*$^{iΔTC/ΔTC}$ GFP$^{+}$ cells among total retinal ECs, which may reflect slow inactivation of *Rbpj*[8] and redundant functions of *Notch1* and *Notch4* (ref. 45) (Fig. 6g,h).

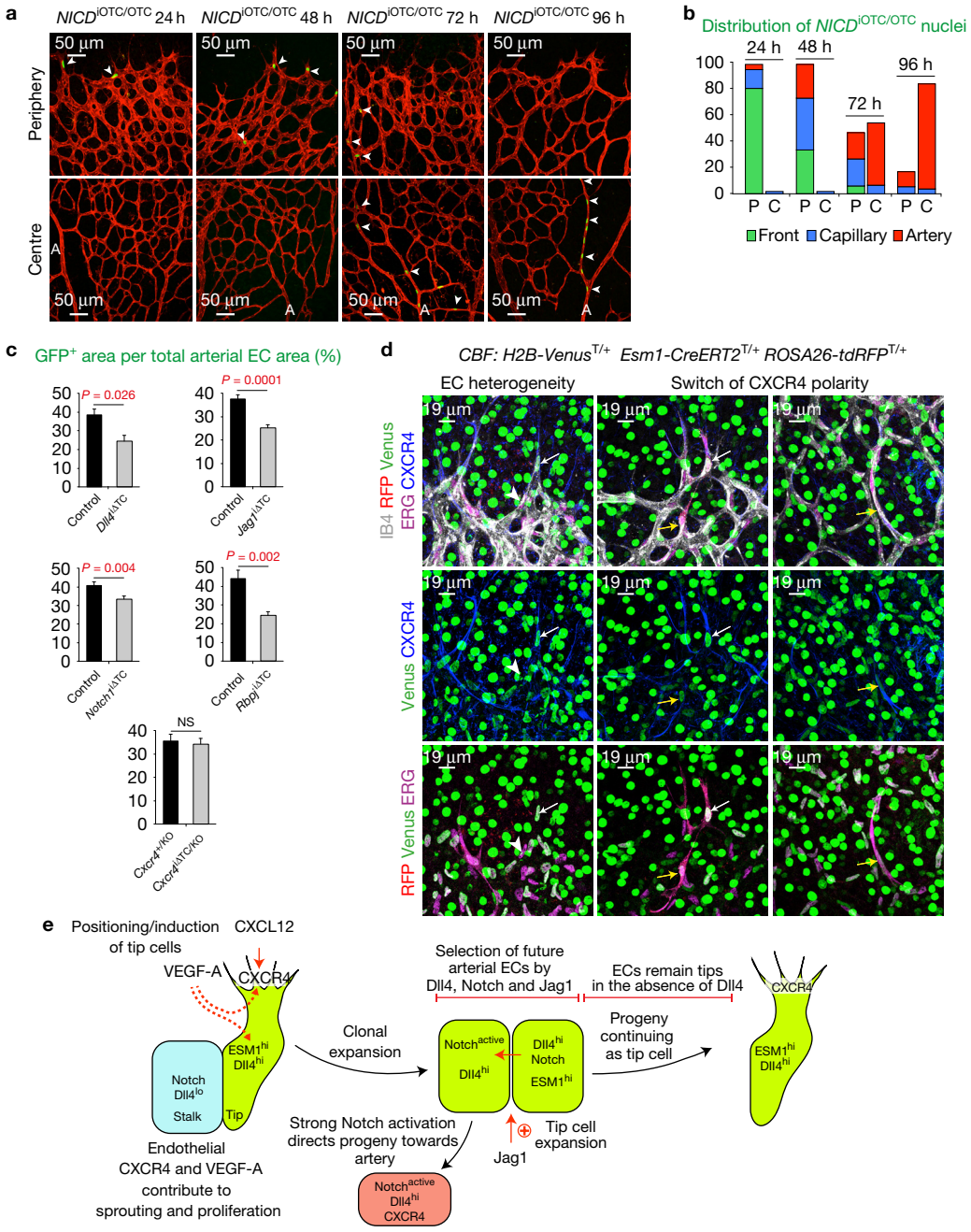


**Figure 8** Notch activation directs tip cell progeny into arteries. (**a**) Confocal images of IB4 (red) and active nuclear NICD (GFP; green) in *NICD*$^{iOTC/OTC}$ (*Esm1-CreERT2*$^{T/+}$ *Gt(ROSA)26Sor*$^{tm1(Notch1)dam}$) retinal vessels at 24 h, 48 h, 72 h and 96 h after 4-OHT administration. Recombined GFP$^{+}$ ECs (white arrowheads) were mainly found in the periphery at the leading front and in the capillary plexus at 24 h and 48 h after 4-OHT administration but predominantly populated arteries (A) at 72 h and 96 h. (**b**) Distribution of GFP$^{+}$ *NICD*$^{iOTC/OTC}$ ECs at 24 h ($n = 5$ retinas), 48 h ($n = 6$ retinas), 72 h ($n = 7$ retinas) and 96 h ($n = 7$ retinas) after 4-OHT injection. Note the significant decrease of GFP$^{+}$ cells from the periphery (P) at 24 h and 48 h and enrichment in arteries of the central plexus (C) between 72 h and 96 h. Total GFP$^{+}$ nuclei distribution from the front area and central plexus was subdivided according to the *NICD*$^{iOTC/OTC}$ EC localization in the leading front, capillaries and arteries. Data represent mean values obtained from two independent 4-OHT injections for each time point. (**c**) Quantification of recombined GFP$^{+}$ cells per total arterial EC area for *Dll4*$^{i\Delta TC/\Delta TC}$ ($n = 8$ control and 8 *Dll4*$^{i\Delta TC/\Delta TC}$ retinas), *Jag1*$^{i\Delta TC/\Delta TC}$ ($n = 8$ control and 8 *Jag1*$^{i\Delta TC/\Delta TC}$ retinas) and *Notch1*$^{i\Delta TC/\Delta TC}$ ($n = 9$ control and 13 *Notch1*$^{i\Delta TC/\Delta TC}$ retinas) at 96 h after 4-OHT injection. Reduced arterial contribution of GFP$^{+}$ ECs was also seen in the *Rbpj*$^{i\Delta TC/\Delta TC}$ ($n = 8$ *Rbpj*$^{i\Delta TC/+}$ control and 6 *Rbpj*$^{i\Delta TC/\Delta TC}$ retinas) at 72 h but not in the *Cxcr4*$^{i\Delta TC/KO}$ ($n = 12$ *Cxcr4*$^{+/KO}$ control and 10 *Cxcr4*$^{i\Delta TC/KO}$ retinas) vasculature at 96 h after 4-OHT injection. Data represent mean ± s.e.m. *P* values, two-tailed unpaired *t*-test. NS, not significant. (**d**) Maximum intensity projections of IB4 (white), CXCR4 (blue), ERG (purple), RFP (red, ESM1 recombined cells) and active endogenous Notch (YFP/Venus, green) immunostaining in *CBF:H2B-Venus* Notch reporter (*Esm1-CreERT2*$^{T/+}$ *CBF:H2B-Venus*$^{T/+}$ *ROSA26-tdRFP*$^{T/+}$). The white arrows point to ECs with high Notch activity while the white arrowheads indicate ERG$^{+}$ cells with no detectable Notch reporter signal. The yellow arrows indicate *Esm1-CreERT2*-labelled ERG$^{+}$ ECs found away from the capillary front with reversed CXCR4 polarization. (**e**) Model depicting the role of endothelial tip cells (green) as progenitors of arterial ECs (red) and the regulation by CXCL12–CXCR4, Jag1 and Dll4–Notch signalling.

Next, we tracked GFP$^+$ *Dll4*$^{i\Delta TC/\Delta TC}$ *R26-mTmG* ECs after *Esm1-CreERT2*-mediated inactivation of *Dll4*. GFP$^+$ *Dll4*$^{i\Delta TC/\Delta TC}$ ECs were enriched at P6 after a single 4-OHT injection and successful loss of Dll4 in GFP$^+$ ECs was validated by immunohistochemistry (Fig. 7a,b and Supplementary Fig. 7a,b). *Dll4*$^{i\Delta TC/\Delta TC}$ ECs were significantly enriched in sprouts indicating that there is no cell-autonomous requirement for Dll4 in tip cells (Fig. 7b). Moreover, GFP$^+$ Dll4-deficient tip cells were frequently seen in direct proximity of unrecombined stalk cells exhibiting Dll4 immunostaining (Fig. 7c). *Esm1-CreERT2*-mediated loss of Dll4 also led to the emergence of extensive protrusions in recombined ECs, which was most evident in *Dll4*$^{i\Delta TC/\Delta TC}$ mutants at 48 h after 4-OHT treatment (Supplementary Fig. 7a). Similar to pan-endothelial *Dll4* mutants, CXCR4 was upregulated in the *Dll4*$^{i\Delta TC/\Delta TC}$ vasculature, whereas immunostaining of Jagged1 was locally reduced (Supplementary Fig. 7c,d). When the role of Jagged1 was investigated with *Esm1-CreERT2* transgenic mice, the abundance of *Jag1*-deficient cells within sprouts was significantly reduced at 96 h (Fig. 7d,e). The loss of Jagged1 protein in GFP$^+$ ECs was confirmed by immunostaining (Fig. 7f). CXCR4 and Dll4 immunostaining was comparable in *Jag1*$^{i\Delta TC/\Delta TC}$ and control retinas (Supplementary Fig. 7e,f). These results show that loss of *Dll4* did not compromise the ability of ECs to function as tip cells, whereas the abundance of *Jag1*-deficient cells was reduced in sprouts.

### Notch activation specifies pre-arterial, tip-cell-derived ECs

To investigate the effect of Notch activation (that is, NICD expression) in ESM1$^+$ tip cells, we combined *Esm1-CreERT2* transgenic mice and *Gt(ROSA)26Sor*$^{tm1(Notch1)Dam}$ homozygotes (*NICD*$^{iOTC/OTC}$). Cre-dependent NICD expression was detected by the presence of nuclear-localized GFP encoded by the *Gt(ROSA)26Sor*$^{tm1(Notch1)Dam}$ allele[46]. Analysis of the resulting mutants showed that GFP$^+$ *NICD*$^{iOTC/OTC}$ ECs were abundant at the front and in capillaries at 24 or 48 h after 4-OHT administration, whereas GFP$^+$ cells were increasingly confined to arteries in both the central and peripheral retina after 72 and 96 h (Fig. 8a,b and Supplementary Fig. 8a). GFP$^+$ *NICD*$^{iOTC/OTC}$ ECs expressed Dll4 and showed CXCR4 immunostaining (Supplementary Fig. 8a–c). Further supporting an important role of Dll4–Notch signalling in the specification of arterial ECs at the angiogenic front, GFP$^+$ *Dll4*$^{i\Delta TC/\Delta TC}$, *Jag1*$^{i\Delta TC/\Delta TC}$, *Notch1*$^{i\Delta TC/\Delta TC}$ and *Rbpj*$^{i\Delta TC/\Delta TC}$ ECs were significantly less abundant in arteries than control ECs, whereas arterial contribution was not significantly different between GFP$^+$ *Cxcr4*$^{i\Delta TC/KO}$ mutant and *Cxcr4*$^{+/KO}$ control ECs (Fig. 8c and Supplementary Fig. 8d).

An improved immunostaining protocol visualizing active (cleaved) Notch[47] showed the expected labelling of arteries, perivascular cells and a subset of ECs within endothelial sprouts (Supplementary Fig. 8e). NICD-positive ECs were also found within the vascular plexus in proximity of small arterioles. For visualization of Notch signalling in tip-cell-derived ECs, we introduced the *CBF:H2B-Venus*[48] Notch reporter allele into *Esm1-CreERT2* mice carrying the *ROSA26-tdRFP*$^{T/+}$ *Cre* reporter[49]. H2B-Venus-positive and -negative endothelial nuclei (visualized by ERG immunostaining) indicated that ECs were not uniformly labelled due to longevity of the Notch reporter signal (Fig. 8d and Supplementary Fig. 8f). H2B-Venus signal was seen in RFP$^+$ ERG$^+$ CXCR4$^+$ tip cells at the angiogenic front and in tip-cell-derived ECs within the capillary plexus. While CXCR4 labelled the distal endothelial sprouts directed towards the avascular retina, this polarity was reversed within the plexus consistent with the migration of RFP$^+$ ERG$^+$ ECs towards arteries (Fig. 8d and Supplementary Fig. 8f).

These data argue that Notch activation controls an important behavioural switch in tip-cell-derived ECs at the angiogenic front. Cells with high Notch activity are directed into developing arteries, whereas other tip cell progeny—presumably with a lower level of Notch signalling—continue to function as tip cells even in the absence of Dll4. These findings are consistent with the established role of Notch in arterial differentiation[9,50–53].

## DISCUSSION

Our results show that Notch inhibition triggers upregulation of endothelial VEGF-A and CXCR4, which enhances endothelial sprouting and proliferation. ChIP experiments indicate binding of RBPJ, which can act as a transcriptional activator or repressor[54,55], to *Vegfa*, which may regulate expression of the growth factor directly, whereas *Cxcr4* expression appears to be controlled by VEGF-A/VEGFR2 signalling. Thus, endothelial VEGF-A is not only a survival signal[28] but also a critical regulator of vascular growth. Strikingly, EC-specific *Vegfr2* mutants display very severe vascular defects[5,8] and substantial EC apoptosis but still respond to Notch inhibition. As therapeutic VEGF-A/VEGFR2 inhibition is limited by factors such as compound efficiency, kinetics and side effects, the impact of low or impaired endothelial Notch signalling in this context deserves further investigation.

VEGF-A and Dll4–Notch signalling has been implicated in the specification of endothelial tip cells and in positional changes within sprouts[3,4,6,7,9,14]. *Esm1-CreERT2*-mediated marking of tip cells indicates that labelled ECs and their progeny can retain their leading position in sprouts for prolonged time periods *in vivo*. It was also suggested, in critical parts relying on data obtained from *in vitro* assays, that Dll4 mediates competitive interactions between ECs striving for the tip position[7,14], whereas our results show that Dll4-deficient tip cells can lead sprouts and even gain a competitive advantage over unrecombined ECs *in vivo*. Thus, ESM1$^+$ tip cells appear intrinsically primed to mediate sprouting processes (Fig. 8e). An independent study has made similar findings in the developing zebrafish embryo. Tip cells lacking dll4 can acquire and retain the leading position in vessel sprouts and also display substantial Notch activation, which was demonstrated by *in vivo* live imaging of transgenic reporter animals[56]. These findings are consistent with our conclusion that Dll4–Notch signaling interactions occur among the tip cell progeny to control the specification of future arterial ECs. In our model, ECs are primed by Notch activation at the angiogenic front, migrate into the vessel plexus and mediate artery growth (Fig. 8e). This is consistent with our previous finding that Notch activity is not required within the postnatal arterial endothelium[39], whereas pan-endothelial Notch pathway mutants exhibit profound arterial defects[4,19,39,57,58]. Arterial incorporation of former tip cells was also observed during zebrafish tail fin regeneration[42]. Vein-derived tip cells turn around and move into expanding arteries but not veins. This migration is collective and was rescued by wild-type cells in mosaic *cxcr4a* loss-of-function mutants. Cooperative behaviour may also explain why retinal *Cxcr4*$^{i\Delta TC/KO}$ ECs had an impaired ability to lead sprouts, whereas arterial incorporation was not significantly altered. On the basis of the evidence presented

here, we propose that signalling processes in angiogenic sprouts are directly coupled to artery formation (Fig. 8e), which might coordinate vessel growth and arterial network enlargement. □

## METHODS

Methods, including statements of data availability and any associated accession codes and references, are available in the online version of this paper.

*Note: Supplementary Information is available in the online version of the paper*


### ACKNOWLEDGEMENTS

We thank G. de Luxán for help with the active NICD immunostaining protocol and H. J. Fehling (Institute of Immunology, University Clinics Ulm, Germany) for providing ROSA26$^{RFP}$ mice. The Max Planck Society, the University of Münster, the Cells in Motion (CiM) graduate school, the DFG Research Unit 2325 and the DFG cluster of excellence 'Cells in Motion' have supported this study.


### AUTHOR CONTRIBUTIONS

M.E.P., S.F.R. and R.H.A. designed the study. M.E.P., I.S., T.A. and F.B. performed experiments, B.D.G., F.F. and T.B. performed and analysed ChIP experiments, M.E. initiated the NICD rescue experiments, D.B. performed the *R26R-Confetti* clonal expansion and part of the *Rbpj*$^{i\Delta TC}$ experiments, H.P. and U.H.L. contributed with image acquisition and quantification, M.S. performed the flow cytometry sorting of retinal ECs, S.F.R., T.N. and N.F. generated mutant mice, and M.E.P. and R.H.A. wrote the manuscript.

### COMPETING FINANCIAL INTERESTS

The authors declare no competing financial interests.


Published online at http://dx.doi.org/10.1038/ncb3555




1. Koch, S. & Claesson-Welsh, L. Signal transduction by vascular endothelial growth factor receptors. *Cold Spring Harb. Perspect. Med.* **2,** a006502 (2012).
2. Ferrara, N., Gerber, H. P. & LeCouter, J. The biology of VEGF and its receptors. *Nat. Med.* **9,** 669–676 (2003).
3. Lobov, I. B. *et al.* Delta-like ligand 4 (Dll4) is induced by VEGF as a negative regulator of angiogenic sprouting. *Proc. Natl Acad. Sci. USA* **104,** 3219–3224 (2007).
4. Hellstrom, M. *et al.* Dll4 signalling through Notch1 regulates formation of tip cells during angiogenesis. *Nature* **445,** 776–780 (2007).
5. Zarkada, G., Heinolainen, K., Makinen, T., Kubota, Y. & Alitalo, K. VEGFR3 does not sustain retinal angiogenesis without VEGFR2. *Proc. Natl Acad. Sci. USA* **112,** 761–766 (2015).
6. Suchting, S. *et al.* The Notch ligand Δ-like 4 negatively regulates endothelial tip cell formation and vessel branching. *Proc. Natl Acad. Sci. USA* **104,** 3225–3230 (2007).
7. Jakobsson, L. *et al.* Endothelial cells dynamically compete for the tip cell position during angiogenic sprouting. *Nat. Cell Biol.* **12,** 943–953 (2010).
8. Benedito, R. *et al.* Notch-dependent VEGFR3 upregulation allows angiogenesis without VEGF-VEGFR2 signalling. *Nature* **484,** 110–114 (2012).
9. Siekmann, A. F. & Lawson, N. D. Notch signalling limits angiogenic cell behaviour in developing zebrafish arteries. *Nature* **445,** 781–784 (2007).
10. Tammela, T. *et al.* Blocking VEGFR-3 suppresses angiogenic sprouting and vascular network formation. *Nature* **454,** 656–660 (2008).
11. Benedito, R. *et al.* The Notch ligands Dll4 and Jagged1 have opposing effects on angiogenesis. *Cell* **137,** 1124–1135 (2009).
12. Pedrosa, A. R. *et al.* Endothelial Jagged1 antagonizes Dll4 regulation of endothelial branching and promotes vascular maturation downstream of Dll4/Notch1. *Arterioscler. Thromb. Vasc. Biol.* **35,** 1134–1146 (2015).
13. Kangsamaksin, T. *et al.* NOTCH decoys that selectively block DLL/NOTCH or JAG/NOTCH disrupt angiogenesis by unique mechanisms to inhibit tumor growth. *Cancer Discov.* **5,** 182–197 (2015).
14. Arima, S. *et al.* Angiogenic morphogenesis driven by dynamic and heterogeneous collective endothelial cell movement. *Development* **138,** 4763–4776 (2011).
15. Bentley, K., Gerhardt, H. & Bates, P. A. Agent-based simulation of notch-mediated tip cell selection in angiogenic sprout initialisation. *J. Theor. Biol.* **250,** 25–36 (2008).
16. Bentley, K., Mariggi, G., Gerhardt, H. & Bates, P. A. Tipping the balance: robustness of tip cell selection, migration and fusion in angiogenesis. *PLoS Comput. Biol.* **5,** e1000549 (2009).
17. Bentley, K. *et al.* The role of differential VE-cadherin dynamics in cell rearrangement during angiogenesis. *Nat. Cell Biol.* **16,** 309–321 (2014).
18. Boas, S. E. & Merks, R. M. Tip cell overtaking occurs as a side effect of sprouting in computational models of angiogenesis. *BMC Syst. Biol.* **9,** 86 (2015).
19. Sorensen, I., Adams, R. H. & Gossler, A. DLL1-mediated Notch activation regulates endothelial identity in mouse fetal arteries. *Blood* **113,** 5680–5688 (2009).
20. Napp, L. C. *et al.* Extrinsic Notch ligand Δ-like 1 regulates tip cell selection and vascular branching morphogenesis. *Circ. Res.* **110,** 530–535 (2012).
21. Tachibana, K. *et al.* The chemokine receptor CXCR4 is essential for vascularization of the gastrointestinal tract. *Nature* **393,** 591–594 (1998).
22. Ara, T., Tokoyoda, K., Okamoto, R., Koni, P. A. & Nagasawa, T. The role of CXCL12 in the organ-specific process of artery formation. *Blood* **105,** 3155–3161 (2005).
23. Ding, B. S. *et al.* Divergent angiocrine signals from vascular niche balance liver regeneration and fibrosis. *Nature* **505,** 97–102 (2014).
24. Strasser, G. A., Kaminker, J. S. & Tessier-Lavigne, M. Microarray analysis of retinal endothelial tip cells identifies CXCR4 as a mediator of tip cell morphology and branching. *Blood* **115,** 5102–5110 (2010).
25. Unoki, N. *et al.* SDF-1/CXCR4 contributes to the activation of tip cells and microglia in retinal angiogenesis. *Invest. Ophthalmol. Vis. Sci.* **51,** 3362–3371 (2010).
26. Stone, J. *et al.* Development of retinal vasculature is mediated by hypoxia-induced vascular endothelial growth factor (VEGF) expression by neuroglia. *J. Neurosci.* **15,** 4738–4747 (1995).
27. Detmar, M. *et al.* Hypoxia regulates the expression of vascular permeability factor/vascular endothelial growth factor (VPF/VEGF) and its receptors in human skin. *J. Invest. Dermatol.* **108,** 263–268 (1997).
28. Lee, S. *et al.* Autocrine VEGF signaling is required for vascular homeostasis. *Cell* **130,** 691–703 (2007).
29. Domigan, C. K. *et al.* Autocrine VEGF maintains endothelial survival through regulation of metabolism and autophagy. *J. Cell Sci.* **128,** 2236–2248 (2015).
30. Fan, J. *et al.* Crim1 maintains retinal vascular stability during development by regulating endothelial cell Vegfa autocrine signaling. *Development* **141,** 448–459 (2014).
31. del Toro, R. *et al.* Identification and functional analysis of endothelial tip cell-enriched genes. *Blood* **116,** 4025–4033 (2010).
32. Rocha, S. F. *et al.* Esm1 modulates endothelial tip cell behavior and vascular permeability by enhancing VEGF bioavailability. *Circ. Res.* **115,** 581–590 (2014).
33. Han, H. *et al.* Inducible gene knockout of transcription factor recombination signal binding protein-J reveals its essential role in T versus B lineage decision. *Int. Immunol.* **14,** 637–645 (2002).
34. Diaz-Trelles, R. *et al.* Notch-independent RBPJ controls angiogenesis in the adult heart. *Nat. Commun.* **7,** 12088 (2016).
35. Taylor, K. L., Henderson, A. M. & Hughes, C. C. Notch activation during endothelial cell network formation *in vitro* targets the basic HLH transcription factor HESR-1 and downregulates VEGFR-2/KDR expression. *Microvasc. Res.* **64,** 372–383 (2002).
36. Williams, C. K., Li, J. L., Murga, M., Harris, A. L. & Tosato, G. Up-regulation of the Notch ligand Delta-like 4 inhibits VEGF-induced endothelial cell function. *Blood* **107,** 931–939 (2006).
37. Harrington, L. S. *et al.* Regulation of multiple angiogenic pathways by Dll4 and Notch in human umbilical vein endothelial cells. *Microvasc. Res.* **75,** 144–154 (2008).
38. Holderfield, M. T. & Hughes, C. C. Crosstalk between vascular endothelial growth factor, notch, and transforming growth factor-β in vascular morphogenesis. *Circ. Res.* **102,** 637–652 (2008).
39. Ehling, M., Adams, S., Benedito, R. & Adams, R. H. Notch controls retinal blood vessel maturation and quiescence. *Development* **140,** 3051–3061 (2013).
40. Liu, Q. *et al.* Genetic targeting of sprouting angiogenesis using Apln-CreER. *Nat. Commun.* **6,** 6020 (2015).
41. Muzumdar, M. D., Tasic, B., Miyamichi, K., Li, L. & Luo, L. A global double-fluorescent Cre reporter mouse. *Genesis* **45,** 593–605 (2007).
42. Xu, C. *et al.* Arteries are formed by vein-derived endothelial tip cells. *Nat. Commun.* **5,** 5758 (2014).
43. Schepers, A. G. *et al.* Lineage tracing reveals Lgr5$^{+}$ stem cell activity in mouse intestinal adenomas. *Science* **337,** 730–735 (2012).
44. Ridgway, J. *et al.* Inhibition of Dll4 signalling inhibits tumour growth by deregulating angiogenesis. *Nature* **444,** 1083–1087 (2006).
45. Krebs, L. T. *et al.* Notch signaling is essential for vascular morphogenesis in mice. *Genes Dev.* **14,** 1343–1352 (2000).
46. Murtaugh, L. C., Stanger, B. Z., Kwan, K. M. & Melton, D. A. Notch signaling controls multiple steps of pancreatic differentiation. *Proc. Natl Acad. Sci. USA* **100,** 14920–14925 (2003).
47. Del Monte, G., Grego-Bessa, J., Gonzalez-Rajal, A., Bolos, V. & De La Pompa, J. L. Monitoring Notch1 activity in development: evidence for a feedback regulatory loop. *Dev. Dynam.* **236,** 2594–2614 (2007).
48. Nowotschin, S., Xenopoulos, P., Schrode, N. & Hadjantonakis, A. K. A bright single-cell resolution live imaging reporter of Notch signaling in the mouse. *BMC Dev. Biol.* **13,** 15 (2013).
49. Luche, H., Weber, O., Nageswara Rao, T., Blum, C. & Fehling, H. J. Faithful activation of an extra-bright red fluorescent protein in "knock-in" Cre-reporter mice ideally suited for lineage tracing studies. *Eur. J. Immunol.* **37,** 43–53 (2007).
50. Lawson, N. D. *et al.* Notch signaling is required for arterial-venous differentiation during embryonic vascular development. *Development* **128,** 3675–3683 (2001).
51. Zhong, T. P., Childs, S., Leu, J. P. & Fishman, M. C. Gridlock signalling pathway fashions the first embryonic artery. *Nature* **414,** 216–220 (2001).

52. Duarte, A. *et al*. Dosage-sensitive requirement for mouse Dll4 in artery development. *Genes Dev.* **18,** 2474–2478 (2004).
53. Carlson, T. R. *et al*. Endothelial expression of constitutively active Notch4 elicits reversible arteriovenous malformations in adult mice. *Proc. Natl Acad. Sci. USA* **102,** 9884–9889 (2005).
54. Wang, H. *et al*. Genome-wide analysis reveals conserved and divergent features of Notch1/RBPJ binding in human and murine T-lymphoblastic leukemia cells. *Proc. Natl Acad. Sci. USA* **108,** 14908–14913 (2011).
55. Liefke, R. *et al*. Histone demethylase KDM5A is an integral part of the core Notch-RBP-J repressor complex. *Genes Dev.* **24,** 590–601 (2010).
56. Hasan, S. S. *et al*. Endothelial Notch signalling limits angiogenesis via control of artery formation. *Nat. Cell Biol.* **19,** http://dx.doi.org/10.1038/ncb3574 (2017).
57. Limbourg, A. *et al*. Notch ligand Delta-like 1 is essential for postnatal arteriogenesis. *Circ. Res.* **100,** 363–371 (2007).
58. Nielsen, C. M. *et al*. Deletion of Rbpj from postnatal endothelium leads to abnormal arteriovenous shunting in mice. *Development* **141,** 3782–3792 (2014).

DOI: 10.1038/ncb3555

## METHODS

**Genetic mouse models and pharmacological treatments.** For immunostaining of wild-type retinas, C57BL/6J pups were used. To inactivate *Dll4* in the postnatal endothelium *Dll4*$^{lox/lox}$ mice[59] and *Pdgfb-iCre*$^{T/+}$ transgenic mice[60] were interbred. *Pdgfb-iCre*$^{T/+}$ *Dll4*$^{lox/lox}$ males were mated with *Dll4*$^{lox/lox}$ females to generate litters for analysis. For Cre activation, offspring were injected every day, from P1 to P3, with 50 µg tamoxifen (Sigma-Aldrich, T5648)[61] and analysed at P6.

To induce expression of active NOTCH on a *Dll4* endothelial-specific loss-of-function-background, *Gt(ROSA)26Sor*$^{tm1(Notch1)Dam/J}$ (ref. 46) homozygous mice, carrying an inducible transgene for Notch1 intracellular domain overexpression (NICD), were interbred with *Pdgfb-iCre*$^{T/+}$ *Dll4*$^{lox/lox}$ mice. Pups obtained from interbreeding of *Dll4*$^{lox/lox}$ *NICD*$^{lox/+}$ and *Pdgfb-iCre*$^{T/+}$ *Dll4*$^{lox/lox}$ *NICD*$^{lox/+}$ mice were injected with 50 µg tamoxifen at P2 and P3 and analysed at P6.

For combined inactivation of *Dll1* and *Dll4* in ECs, *Dll1*$^{lox/lox}$ mice[62] were interbred with *Dll4*$^{lox/lox}$ (ref. 59) and *Pdgfb-iCre*$^{T/+}$ *Dll4*$^{lox/lox}$ mice. Offspring obtained from interbreeding of *Dll1*$^{lox+}$ *Dll4*$^{lox/lox}$ and *Pdgfb-iCre*$^{T/+}$ *Dll1*$^{lox+}$ *Dll4*$^{lox/lox}$ mice were daily injected from P1 to P3 with 50 µg tamoxifen and retinas were analysed at P6.

To delete *Vegfa* in the postnatal endothelium, *Vegfa*$^{lox/lox}$ mice[63] and *Pdgfb-iCre*$^{T/+}$ *Vegfa*$^{lox/lox}$ mice were mated. Pups were injected daily from P1 to P3 with 50 µg tamoxifen and analysed at P6.

For EC-specific *Flk1* loss-of-function experiments, we interbred *Flk1* knockout heterozygous males[64], carrying the *Pdgfb-iCre*$^{T/+}$ transgene (*Pdgfb-iCre*$^{T/+}$ *Flk1*$^{KO/+}$) with *Flk1*$^{lox/lox}$ females[65]. To avoid lethality of mutant offspring, pups were injected at P1 and P2 with 50 µg tamoxifen prior to analysis at P6.

To inactivate *Cxcr4* in the postnatal endothelium, *Cxcr4*$^{lox/lox}$ females[66] and *Pdgfb-iCre*$^{T/+}$ *Cxcr4*$^{lox/lox}$ male mice were mated. Alternatively, *Cxcr4* knockout heterozygote[21] males carrying the *Cdh5(PAC)CreERT2*$^{T/+}$ transgene[67] (*Cdh5-CreERT2*$^{T/+}$*Cxcr4*$^{+/KO}$) were interbred with *Cxcr4*$^{lox/lox}$ females. The generated mutants (*Cxcr4*$^{i\Delta EC/KO}$) were compared with control (*Cxcr4*$^{lox/+}$) or heterozygous knockout (*Cxcr4*$^{+/KO}$) mice, as described in the text and figure legends. Offspring were daily injected from P1 to P3 with 50 µg tamoxifen and analysed at P6.

For EC-specific *Rbpj* loss-of-function experiments, we mated *Rbpj*$^{lox/lox}$ (ref. 33) and *Pdgfb-iCre*$^{T/+}$ *Rbpj*$^{lox/lox}$ mice. Offspring were daily injected from P1 to P3 with 50 µg tamoxifen and retinas were analysed at P7.

For combined inactivation of *Cxcr4* and *Rbpj* in ECs, *Pdgfb-iCre*$^{T/+}$ *Cxcr4* $^{+/KO}$ *Rbpj*$^{lox/lox}$ males were interbred with *Cxcr4*$^{lox/lox}$ *Rbpj* $^{lox/lox}$ females. Offspring were daily injected from P1 to P3 with 50 µg tamoxifen and analysed at P6.

For combined deletion of *Cxcr4* and *Dll4* in ECs, *Pdgfb-iCre*$^{T/+}$ *Cxcr4*$^{lox/+}$ *Dll4*$^{lox/lox}$ and *Cxcr4*$^{lox/+}$ *Dll4*$^{lox/lox}$ mice were mated. To avoid fusion of sprouts seen after prolonged inactivation of *Dll4*, offspring were injected daily from P3 to P5 with 50 µg tamoxifen and retinas were analysed at P6.

*Cxcl12-GFP* mice[68] were purchased from MMRRC (stock number: 000277-MU).

For overexpression of active NOTCH in endothelium, *Gt(ROSA)26Sor*$^{tm1(Notch1)Dam/J}$ homozygous mice[46] (*NICD*$^{lox/lox}$) were interbred with *NICD*$^{lox/lox}$ *Pdgfb-iCre*$^{T/+}$ mice. Pups were injected daily from P1 to P3 with 50 µg tamoxifen and analysed at P6.

For lineage tracing analysis of tip cells[32], *Esm1-CreERT2*$^{T/+}$ transgenics were combined with *R26-mTmG*$^{T/T}$ Cre reporter mice[41]. The generated offspring were injected with 12.5 µg of 4-hydroxytamoxifen (4-OHT) (Sigma, H7904) at time points described in the text and legends and analysed at P6. For clonal expansion analysis, *Esm1-CreERT2*$^{T/+}$ transgenics were combined with *R26R-Confetti*$^{T/+}$ reporter mice[43]. The resulting pups were injected with 50 µg tamoxifen at P1 and P2 and analysed at P6.

To inactivate *Cxcr4* in tip cells, *Esm1-CreERT2*$^{T/+}$ *Cxcr4*$^{+/KO}$ and *Cxcr4*$^{lox/+}$ *R26-mTmG*$^{T/T}$ mice were interbred. The resulting offspring were injected once at P2 with 12.5 µg of 4-OHT and Cre$^{+}$ mice were analysed at P6.

To inactivate *Dll4*, *Jag1* or *Notch1* in tip cells, mice heterozygous for floxed *Dll4* (ref. 59), *Jag1* (ref. 69) or Notch1 (ref. 70), in combination with *R26-mTmG*$^{T/T}$, were interbred with mice double heterozygous for *Dll4* (*Dll4*$^{lox/+}$), *Jag1* (*Jag1*$^{lox/+}$) or *Notch1* (*Notch1*$^{lox/+}$) and the *Esm1-CreERT2*$^{T/+}$ transgene. The resulting offspring were injected once at P2 with 12.5 µg of 4-OHT and Cre$^{+}$ mice were analysed at P6.

To inactivate *Rbpj* in ESM1$^{+}$ cells, *Rbpj*$^{lox/lox}$ *R26-mTmG*$^{T/T}$ and *Rbpj*$^{lox/+}$ *Esm1-CreERT2*$^{T/+}$ mice were interbred. Their pups were injected with 50 µg of 4-OHT at P2 and P3 and analysed at P5.

*Gt(ROSA)26Sor*$^{tm1(Notch1)Dam/J}$ (ref. 46) is a transgene inserted into the *ROSA26* locus. As homozygotes are required to obtain robust NICD overexpression, recombined ECs were identified by nuclear GFP expression under the control of an IRES sequence in the *Gt(ROSA)26Sor*$^{tm1(Notch1)Dam/J}$ locus. *Esm1-CreERT2*$^{T/+}$ *NICD*$^{lox/lox}$ and *NICD*$^{lox/lox}$ mice were mated and the resulting offspring were injected once at P2, P3, P4 or P5 with 12.5 µg of 4-OHT before analysis at P6.

For visualization of active endogenous Notch activity and tip cell-derived ECs, *CBF:H2B-Venus*$^{T/+}$ (ref. 48) and *Esm1-CreERT2*$^{T/+}$ double heterozygous males (*Esm1-CreERT2*$^{T/+}$ *CBF:H2B-Venus*$^{T/+}$) were interbred with *ROSA26-tdRFP*$^{T/T}$ Cre reporter females[49]. *Esm1-CreERT2*$^{T/+}$ *CBF:H2B-Venus*$^{T/+}$ *ROSA26-tdRFP*$^{T/+}$ pups were injected once at P4 with 12.5 µg of 4-OHT before analysis at P6.

For Notch inhibition, DAPT (Merck Millipore, 565770; 0.1 mg kg$^{-1}$ body weight) or vehicle was injected at P4 and P5 and mice were analysed at P6, 36 h after the first injection.

For CXCR4 inhibition, AMD3100 (Sigma, A5602; 40 µg g$^{-1}$ body weight) was administered twice to *Dll4*$^{i\Delta EC/\Delta EC}$ pups at P5, 12 h and 24 h after 50 µg tamoxifen injection at P4. Pups were analysed at P6, 36 h after tamoxifen treatment.

For VEGF-A inhibition, *NICD*$^{iOEC/OEC}$ and control littermates were injected with tamoxifen from P1 to P3 and with anti-mouse VEGF-A antibody (Bayer, clone G6-23; 1.42 mg ml$^{-1}$, 35 mg kg$^{-1}$ body weight) or a similar volume of PBS at P4 and P5. Pups were analysed at P6, 48 h after the first antibody injection.

All animal experiments were performed in compliance with the relevant laws and institutional guidelines, were approved by local animal ethics committees and were conducted at the University of Münster and the MPI for Molecular Biomedicine with permissions granted by the Landesamt für Natur, Umwelt und Verbraucherschutz (LANUV) of North Rhine-Westphalia. Animals were combined in groups for experiments irrespective of their sex.

**Whole-mount immunohistochemistry of mouse retinas.** Retina immunostaining was performed according to a previously published protocol[61] with minor modifications. Eyes were enucleated and fixed in 4% PFA in PBS. Dissected retinas were blocked in block buffer (1% BSA, 0.3% Triton X-100 in PBS) for 30 min at room temperature and rinsed twice with modified Pblec buffer (1 mM $CaCl_2$, 1 mM $MgCl_2$, 1 mM $MnCl_2$, 0.4% Triton X-100 in PBS). Retinas were incubated overnight at 4 °C with isolectin B4 (IB4) and primary antibodies (see Supplementary Table 1) diluted in modified Pblec buffer. The next day, retinas were washed once in block buffer diluted 1:1 with PBS and three times in PBS. Retinas were incubated with Alexa Fluor (AF)-coupled species-specific secondary antibody (Supplementary Table 1) diluted in block buffer for 1.5 h at room temperature. Retinas were further washed as described above and flat-mounted on glass slides using Fluoromount-G (Southern Biotech, 0100-01).

Immunostaining of *Esm1-CreERT2*$^{T/+}$ *CBF:H2B-Venus*$^{T/+}$ *ROSA26-tdRFP*$^{T/+}$ retinas was performed as described above, with some modifications. After the block/permeabilization step, retinas were incubated overnight at 4 °C with rabbit anti-RFP antibody (Supplementary Table 1). The next day, retinas were washed and incubated with AF-546-coupled donkey anti-rabbit secondary antibody diluted in block buffer for 1.5 h at room temperature. Retinas were further washed and incubated for 1.5 h at room temperature with donkey anti-rabbit F(ab)2 fragments (Supplementary Table 1) to prevent excessive cross-talk with the following primary rabbit antibody. After washing, retinas were re-blocked as before and incubated with IB4, chicken anti-GFP, rabbit anti-ERG and rat anti-CXCR4 antibodies overnight at 4 °C. The next day, retinas were washed and incubated with appropriate secondary antibodies (streptavidin-AF-405, donkey anti-chicken-AF-488, donkey anti-rabbit-AF-594 and donkey anti-rat-AF-647) for 1.5 h at room temperature and processed as described above.

All images shown in the figures are representative for the respective staining in at least three mice unless stated otherwise.

**Antigen retrieval for detection of active NICD in mouse retina.** Detection of endogenous active NOTCH1 was performed using the antigen retrieval method described in ref. 47. C57BL/6J eyes were fixed for 30 min at room temperature in 4% PFA in PBS. Sodium citrate solution (10 mM; pH 6.0) was brought to boiling in a plastic container in a microwave oven and dissected retinas were boiled for 15 min (800 W). Alternatively, retinas were incubated for 15 min in 2 ml Eppendorf tubes filled with sodium citrate solution and placed in a water bath at 95 °C. After cooling down for 20–30 min, retinas were washed four times with distilled water and once with PBS, 3 min per washing step. Endogenous peroxidase was quenched with 'killing solution' (1% $H_2O_2$ in 100% methanol) by incubating retinas for 40 min at room temperature. After three PBS washes for 5 min each, retinas were permeabilized twice in 0.3% Triton X-100/PBS for 10 min each. Retinas were then blocked in Histoblock solution (3% BSA, 20 mM $MgCl_2$, 0.3% Triton X-100, 5% goat serum in PBS) for 1 h at room temperature. Retinas were incubated overnight with primary IB4-488-Alexa Fluor-coupled and rabbit anti-cleaved Notch1 Val1744 antibody (Supplementary Table 1) diluted in Histoblock solution. The next day, retinas were washed twice in PBS and in 0.3% Triton X-100/PBS, 5 min per washing step. Retinas were incubated with goat anti-rabbit biotinylated secondary antibody diluted in 5% BSA in PBS for 1 h at room temperature. Subsequently, retinas were washed as before and incubated with ABC solution (Vector, PK-6100) for 1 h at room temperature. Next, retinas were washed twice for 5 min with 0.3% Triton X-100/PBS and were incubated for 5 min at room temperature with freshly prepared TSA-Cy3 working solution (Perkin Elmer, NEL744001KT). After two washes with PBS and 0.3% Triton X-100/PBS retinas were mounted as described before.

***In vivo* EdU labelling and detection.** To analyse EC proliferation, pups were injected intraperitoneally with 50 µl EdU nucleotides (2 mg ml$^{-1}$ in PBS) at P6, 2 h before euthanization. To detect EdU incorporation in retina vasculature Click-iT EdU Imaging Kit was used (Thermo Fisher Scientific, C10340).

**FACS sorting of mouse retinal ECs.** Collagenase solution (200 U ml$^{-1}$) was prepared in DMEM (Gibco, 31053028) from a 10× stock solution containing 1:1:1 mixture of collagenase I (Gibco, 170100-017), collagenase II (Gibco, 17101-015) and collagenase IV (Gibco, 17104-019). Retinas were dissected from freshly collected eyes and digested in collagenase solution by incubation at 37 °C for 40 min. Lysates were transferred on ice and homogenized by pipetting and vortexing. Digested tissue was filtered through a 70 µm cell strainer (Falcon, 352350) and resuspended in DMEM with 10% FCS. Tissue was spun down in a refrigerated centrifuge for 5 min at 300*g*. The pellet was resuspended in antibody solution (Supplementary Table 1) prepared in DMEM with 3% FCS. Cells were stained for 30 min on ice and then washed twice with DMEM containing 3% FCS. Retinal cells were resuspended in DMEM with 3% FCS and treated with DAPI to exclude dead cells. CD31$^{+}$/CD45$^{-}$ cells were sorted using a FACS Canto flow cytometer and analysed using FACSDiva software (BD Bioscience, Version 6.0).

**RNA extraction from isolated retinal ECs and RT–qPCR.** Retinal ECs were sorted in RLT Plus lysis buffer (Qiagen, 1053393) supplemented with β-mercaptoethanol. RNA extraction was performed using RNeasy Plus Micro Kit (Qiagen, 74034). Whole RNA was reverse transcribed and converted to cDNA using the iScript cDNA synthesis kit (Bio-Rad, 170-8890). Taqman primers, FAM-conjugated probes for *Cxcr4*, *Dll4*, *Esm1*, *Hes1*, *Hey1*, *Jag1*, *Nrarp*, *Vegfa* and *Vegfr2* (Supplementary Table 2) and VIC-conjugated probe for *ActB* (employed to normalize gene expression) were used along with TaqMan Gene Expression Master Mix (Applied Biosystems, 4369016) to perform quantitative PCR on the ABI PRISM 7900HT Fast Real-Time PCR System (Applied Biosystem).

For analysis of mRNAs encoding different VEGF-A isoforms from whole retinas of *Dll4*$^{i\Delta EC/\Delta EC}$ and the corresponding control mice, Taqman primers and FAM-conjugated probes for specific VEGF-A isoforms (Supplementary Table 2) were used as described above.

For each group at least five mice, unless otherwise stated, were analysed to obtain the relative expression differences.

**Notch inhibition in MS1 cells.** Murine pancreatic endothelial MS1 (ATCC CRL-2279) cells were cultured according to the manufacturer's instruction. MS1 cells ($4 \times 10^5$) were plated in a 6-well dish 16 h before DAPT (Merck Millipore, 565770; 10 µM final concentration) or the corresponding volume of dimethylsulfoxide was applied in the preconditioned culture medium. Cells were incubated for 3 h at 37 °C and further lysed in RLT plus lysis buffer (Qiagen, 1053393) supplemented with β-mercaptoethanol.

The MS1 cell line used in this study was neither authenticated nor tested for mycoplasma contamination, and is not listed in the database of commonly misidentified cell lines that is maintained by ICLAC and NCBI Biosample.

**Chromatin immunoprecipitation (ChIP).** ChIP experiments were performed essentially as previously described[71]. Murine MS1 cells were fixed in 1% formaldehyde (FMA) for 10 min at room temperature in the culture medium and the reaction was blocked with 1/8 volume of 1 M glycine pH 8.0. Only in the case of the anti-RBPJ ChIPs, cells were first washed twice in PBS, fixed for 1 h at room temperature in 10 mM dimethyladipimate (DMA) in PBS, washed once in PBS and fixed for 30 min at room temperature in 1% FMA. For all ChIP experiments, cells were washed twice with PBS and resuspended in SDS lysis buffer (1% SDS, 10 mM EDTA, 50 mM Tris-HCl pH 8.1). After 10 min of incubation on ice, the cell suspension was sonicated using a sonication device (Covaris System S220 AFA) and the lysate was centrifuged for 10 min at 18,000*g* at 4 °C. The chromatin was diluted with ChIP dilution buffer (0.01% SDS, 1.1% Triton X-100, 1.2 mM EDTA, 16.7 mM Tris-HCl pH 8.1, 167 mM NaCl) and pre-cleared with 30 µl ml$^{-1}$ nProtein A Sepharose 4 Fast Flow ((GE Healthcare, 17-5280-01); pre-saturated with salmon sperm DNA (Invitrogen)) for 30 min at 4 °C. After centrifugation, 50 µl of chromatin was collected as input control and the rest of the chromatin was aliquoted and incubated overnight with the desired antibody (IgG, anti-RBPJ, anti-H3K4me1, anti-H3K4me3, anti-H3K9ac, anti-H3K9me3, anti-H3K27ac, anti-H3K27me3, anti-H3). Antibodies were immobilized with 40 µl Protein A Sepharose 4 Fast Flow (pre-saturated with salmon sperm DNA) for 1 h at 4 °C with shaking. Beads were washed with low-salt washing buffer (0.1% SDS, 1% Triton X-100, 2 mM EDTA, 20 mM Tris-HCl pH 8.1, 150 mM NaCl), high-salt wash buffer (0.1% SDS, 1% Triton X-100, 2 mM EDTA, 20 mM Tris-HCl pH 8.1, 500 mM NaCl), LiCl wash buffer (0.25M LiCl, 1% IGEPAL-CA630, 1 mM EDTA, 10 mM Tris-HCl pH 8.1) and TE buffer (10 mM Tris-HCl, 1 mM EDTA pH 8.0). Chromatin was eluted from beads with Elution Buffer (1% SDS, 0.1M $NaHCO_3$) and crosslinks were reverted at 65 °C overnight in the presence of 180 mM NaCl. Samples were treated with Proteinase K for 1 h at 45 °C and the DNA was purified by phenol/chloroform extraction. After precipitation overnight at −20 °C in the presence of 10 µg of yeast tRNA, 40 µg glycogen and 500 µl 2-propanol, the DNA was washed with 70% ethanol. The DNA was dried, dissolved in TE pH 8.0 and analysed by qPCR. qPCR reactions were assembled with Absolute QPCR ROX Mix (Thermo Scientific AB-1139), gene-specific oligonucleotides and double-dye probes (see Supplementary Table 2) and finally analysed using the StepOnePlus Real-Time PCR System (Applied Biosystem). A region located on chromosome X (chrX:112357567+112357626) was used as a control.

**Image acquisition, processing and statistical analysis.** Dissection of retinas was done under the dissection microscope (Leica M165C, Leica). Overview pictures of retina samples were imaged using a fluorescence microscope (Leica MZ16 F, Leica) coupled to a digital camera (Hamamatsu C4742-95, Hamamatsu). Confocal image acquisition was performed using confocal microscope SP5 (Leica SP5, Leica) and TCS-SP8 (Leica TCS-SP8, Leica). Photoshop and Illustrator (Adobe) software were used for image processing in compliance with *Nature Cell Biology*'s guidelines for digital images. Processing and quantification of vascular parameters was done using Volocity software (Improvision).

Retina vascular parameter analysis was mostly done as previously described[61].

For the quantification of retinal vessel progression overview images (×2.5) of IB4-stained retina vasculature were obtained. The ratio between the length of vessel progression (from optic disc to the edge of the angiogenic front) and the length of retina leaflet (from optic disc to the periphery) was calculated for each retina leaflet. The mean of all leaflet ratios was obtained per retina and compared between mutant and control groups.

For quantification of filopodia and sprouts, high-resolution confocal images (×40) of IB4-labelled retina vasculature were acquired. Three–four pictures on comparable front areas were imaged for each retina. The quantification of filopodia number in each picture was done by calculating the ratio of total number of filopodia counted per angiogenic front vessel length. The mean for each retina was obtained and compared between the mutant and control groups. The quantification of sprouts in each picture was done by calculating the ratio of total number of sprouts counted per angiogenic front line. The mean for each retina was obtained and compared between mutant and control groups.

For the quantification of branching points and EC area, generally four confocal images (×20) of the IB4-labelled capillary plexus (specifically, the area between an artery and a vein) excluding the angiogenic front were acquired for each retina. A capillary plexus field in which the quantification was further carried out was first defined and identically applied to all of the images acquired. The mean for each retina was obtained and compared between mutant and control groups.

For the quantification of proliferating EC nuclei, four high-resolution confocal images (×40) of IB4-, ERG- and EdU-labelled retinal vasculature were acquired between an artery and a vein for each retina. The total number of Erg$^{+}$ nuclei counted was divided by the EC area for each image acquired. The mean for each retina was obtained and compared between mutant and control groups. In addition, double-positive EdU$^{+}$ Erg$^{+}$ EC nuclei were counted and the total number was divided by the EC area calculated for each acquired image. The mean for each retina was obtained and compared between mutant and control groups.

For the quantification of GFP$^{+}$ sprouts per angiogenic front area, lower-magnification confocal images (×10) of IB4- and GFP-stained retinal vessels were acquired for each retina leaflet. Using the Volocity quantification module, the angiogenic front was defined as a region of interest (ROI). ROIs were limited only to the sprouts and the first adjacent stalk cells. The ratio of GFP$^{+}$ area per angiogenic front IB4$^{+}$ EC area was calculated for each retina leaflet and the mean per retina was compared between mutant and control groups.

For quantification of total GFP$^{+}$ EC area per total EC area, the same ×10 images were used. Using the Volocity quantification module, the ratio of total GFP$^{+}$ area per IB4$^{+}$ EC area was calculated for each retina leaflet and the mean per retina was compared between mutant and control groups.

For the quantification of GFP$^{+}$ area per arterial EC area, a minimum of five samples per group were imaged and analysed. Using the Volocity quantification module, the arterial area was defined as a ROI. ROIs were limited only to the main arteries and first order arterial branches. Arteries in damaged areas or at the edge of the imaged region were excluded. The ratio of GFP$^{+}$ area per IB4$^{+}$ arterial EC area was calculated for each retina leaflet and the mean per retina was compared between mutant and control groups.

Signal intensities of VEGF-A or ESM1 immunostainings were quantified using Adobe Photoshop software from four ×40 acquired confocal images per retina. IB4$^{+}$ area and VEGF-A- or ESM1-immunostained areas were examined by pixel number. For vascular-specific expression, specifically stained area in IB4$^{+}$ vasculature was selectively quantified. The mean per retina was obtained and compared between mutant and control groups.

DOI: 10.1038/ncb3555

For quantification of GFP$^+$ *NICD*$^{iOTC/OTC}$ EC distribution between the periphery and the centre at 24 h, 48 h, 72 h or 96 h after Cre-induced recombination, ×20 confocal images were obtained for both peripheral and central retinal regions, which covered the entire retinal vasculature. The total number of GFP$^+$ nuclei per peripheral and central area was quantified for each retina. Furthermore, the GFP$^+$ nuclei from the peripheral area were counted according to their distribution in the leading front (defined as the area to the second branch in the plexus), capillary plexus or arteries extended in the front area. Similarly, the GFP$^+$ nuclei from the central area were counted according to their localization in the capillary plexus or arteries. The ratio of peripheral or central GFP$^+$ nuclei per total GFP$^+$ nuclei was calculated for individual retina and averaged for each time point analysed.

For each group at least five retinas of mutant and corresponding littermate control pups from three litters injected with tamoxifen or 4-OHT, unless otherwise indicated, were quantified for vascular parameters for statistical analysis.

All images shown in the figures are maximum intensity projections and are representative of at least three mice analysed for each genotype unless stated otherwise.

**Statistics and reproducibility.** Statistical analysis was performed using Microsoft Excel with StatPlus software for data analysis or Graphpad Prism 7 software. All data are presented as mean ± s.e.m. or mean ± s.d. (as indicated in the figure legends). Unpaired two-tailed Student's *t*-tests with Welch's correction (variances between groups were not equal) were used to determine statistical significance between two groups. For analysis of the statistical significance of differences between more than two groups, we performed one-way and two-way ANOVA with Tukey's multiple comparison tests to assess statistical significance with a 95% confidence interval. $P < 0.05$ was considered significant unless stated otherwise. No statistical method was used to predetermine sample size. Sample number was chosen according to the previous experiments. Reproducibility was ensured by several independent experiments. The experiments were not randomized and the investigators were not blinded during experiments and outcome assessment. No animals were excluded from analysis. RT–qPCR results obtained from sorted retinal ECs, in which one of the technical duplicates failed to amplify, were excluded from the analysis. Unless otherwise indicated, results are based on three or more independent experiments to guarantee reproducibility of findings.

**Data availability.** Source data for Fig. 5b,c and Supplementary Fig. 5a have been provided as Supplementary Table 3. All other data supporting the findings of this study are available from the corresponding authors on reasonable request.


59. Koch, U. *et al.* Delta-like 4 is the essential, nonredundant ligand for Notch1 during thymic T cell lineage commitment. *J. Exp. Med.* **205,** 2515–2523 (2008).
60. Claxton, S. *et al.* Efficient, inducible Cre-recombinase activation in vascular endothelium. *Genesis* **46,** 74–80 (2008).
61. Pitulescu, M. E., Schmidt, I., Benedito, R. & Adams, R. H. Inducible gene targeting in the neonatal vasculature and analysis of retinal angiogenesis in mice. *Nat. Protoc.* **5,** 1518–1534 (2010).
62. Hozumi, K. *et al.* Delta-like 1 is necessary for the generation of marginal zone B cells but not T cells *in vivo*. *Nat. Immunol.* **5,** 638–644 (2004).
63. Gerber, H. P. *et al.* VEGF is required for growth and survival in neonatal mice. *Development* **126,** 1149–1159 (1999).
64. Ema, M., Takahashi, S. & Rossant, J. Deletion of the selection cassette, but not cis-acting elements, in targeted Flk1-lacZ allele reveals Flk1 expression in multipotent mesodermal progenitors. *Blood* **107,** 111–117 (2006).
65. Haigh, J. J. *et al.* Cortical and retinal defects caused by dosage-dependent reductions in VEGF-A paracrine signaling. *Dev. Biol.* **262,** 225–241 (2003).
66. Tokoyoda, K., Egawa, T., Sugiyama, T., Choi, B. I. & Nagasawa, T. Cellular niches controlling B lymphocyte behavior within bone marrow during development. *Immunity* **20,** 707–718 (2004).
67. Wang, Y. *et al.* Ephrin-B2 controls VEGF-induced angiogenesis and lymphangiogenesis. *Nature* **465,** 483–486 (2010).
68. Gong, S., Kus, L. & Heintz, N. Rapid bacterial artificial chromosome modification for large-scale mouse transgenesis. *Nat. Protoc.* **5,** 1678–1696 (2010).
69. Brooker, R., Hozumi, K. & Lewis, J. Notch ligands with contrasting functions: Jagged1 and Delta1 in the mouse inner ear. *Development* **133,** 1277–1286 (2006).
70. Yang, X. *et al.* Notch activation induces apoptosis in neural progenitor cells through a p53-dependent pathway. *Dev. Biol.* **269,** 81–94 (2004).
71. Oswald, F. *et al.* A phospho-dependent mechanism involving NCoR and KMT2D controls a permissive chromatin state at Notch target genes. *Nucleic Acids Res.* **44,** 4703–4720 (2016).

nature cell biology

DOI: 10.1038/ncb3555

In the format provided by the authors and unedited.

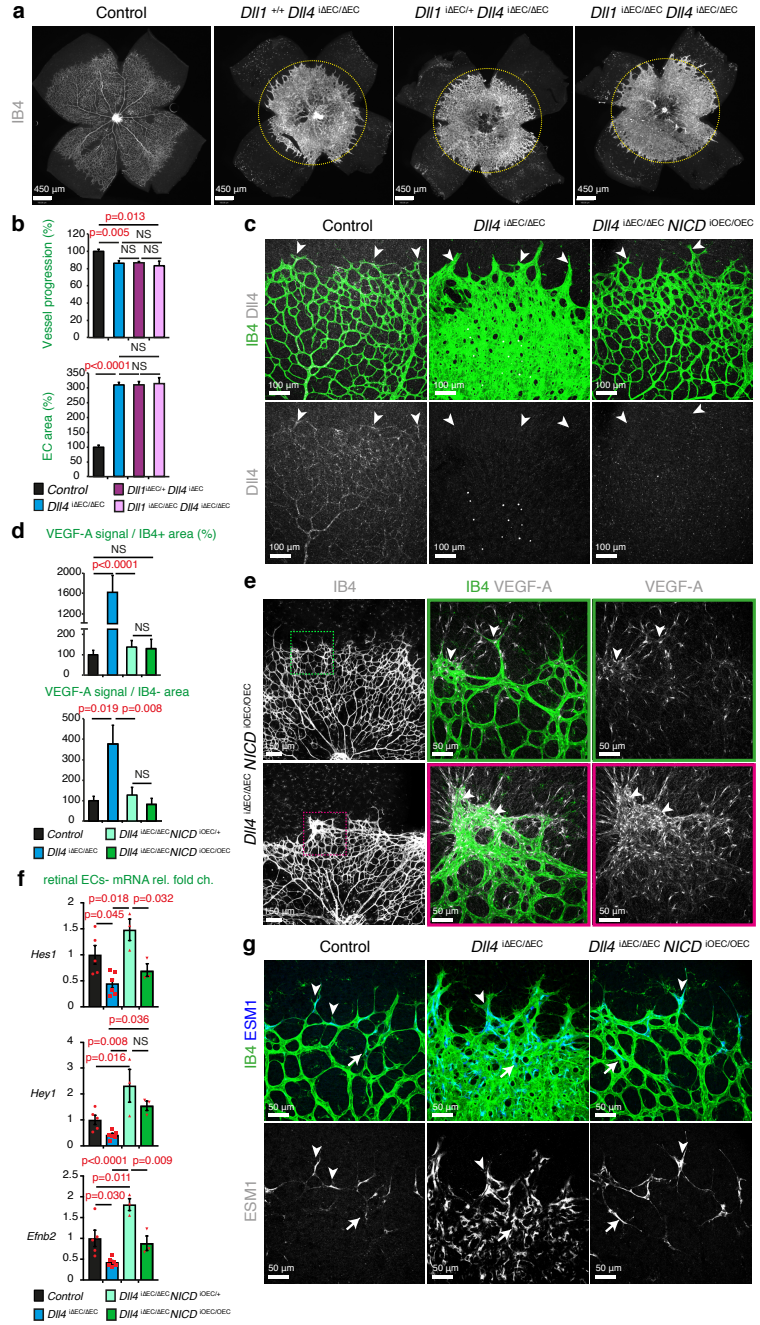


**Supplementary Figure 1** Effect of Notch signalling on CXCR4 and VEGF-A in retinal ECs **a**, Isolectin B4 (IB4, white) stained retinas of *Dll4* $^{iΔEC/ΔEC}$, *Dll1* $^{iΔEC/+}$ *Dll4* $^{iΔEC/ΔEC}$, *Dll1* $^{iΔEC/ΔEC}$ *Dll4* $^{iΔEC/ΔEC}$ and control mice. Circles indicate similar vessel outgrowth.**b**, Quantitation of retinal vessel progression (n=10 control, 8 *Dll4* $^{iΔEC/ΔEC}$, 14 *Dll1* $^{iΔEC/+}$ *Dll4* $^{iΔEC/ΔEC}$ and 6 *Dll1* $^{iΔEC/ΔEC}$ *Dll4* $^{iΔEC/ΔEC}$ retinas) and EC area per field (n=9 control, 5 *Dll4* $^{iΔEC/ΔEC}$, 14 *Dll1* $^{iΔEC/+}$ *Dll4* $^{iΔEC/ΔEC}$ and 6 *Dll1* $^{iΔEC/ΔEC}$ *Dll4* $^{iΔEC/ΔEC}$ retinas). Data represent mean ± s.e.m. *P* values, one-way ANOVA with Tukey's multiple comparison post-hoc test. **c**, Dll4 (white) and IB4 (green) whole-mount staining of control, *Dll4* $^{iΔEC/ΔEC}$ and *Dll4* $^{iΔEC/ΔEC}$ *NICD* $^{iOEC/OEC}$ retinas. Endothelial Dll4 protein can be seen in control but not in mutant samples (arrowheads). **d**, Quantitative analysis of VEGF-A immunosignal in IB4-labelled vessels and total retinas of the indicated mutants at P6 (n=8 control, 5 *Dll4* $^{iΔEC/ΔEC}$, 6 *Dll4* $^{iΔEC/ΔEC}$ *NICD* $^{iOEC/+}$ and 5 *Dll4* $^{iΔEC/ΔEC}$ *NICD* $^{iOEC/OEC}$ retinas). Increased VEGF-A levels in *Dll4* $^{iΔEC/ΔEC}$ ECs were normalized after expression of active Notch. Data represent mean ± s.e.m. *P* values, one-way ANOVA with Tukey's multiple comparison post-hoc test. **e**, Representative images of VEGF-A protein in *Dll4* $^{iΔEC/ΔEC}$ *NICD* $^{iOEC/OEC}$ retinas. ECs were visualized by IB4. Images on the right and in centre depict higher magnifications of insets. Rescue efficiency correlates with endothelial VEGF-A expression (arrowheads). **f**, RT-qPCR analysis of *Hes1*, *Hey1* and *Efnb2* transcripts in sorted retinal ECs of the indicated mutants and littermate controls (n=5 control, 6 *Dll4* $^{iΔEC/ΔEC}$, 3 *Dll4* $^{iΔEC/ΔEC}$ *NICD* $^{iOEC/+}$ and 3 *Dll4* $^{iΔEC/ΔEC}$ *NICD* $^{iOEC/OEC}$ mice from two independent tamoxifen injections). Notch target gene upregulation in *Dll4* $^{iΔEC/ΔEC}$ *NICD* $^{iOEC/+}$ ECs was reduced close to control expression in *Dll4* $^{iΔEC/ΔEC}$ *NICD* $^{iOEC/OEC}$ ECs. Data represent mean ± s.e.m. *P* values, one-way ANOVA with Tukey's multiple comparison post-hoc test. Comparisons where *P* value was not shown are not significant. **g**, Elevated ESM1 (blue/white) in IB4-stained (green) *Dll4* $^{iΔEC/ΔEC}$ ECs relative to control littermates. Arrowheads mark ESM1+ sprouts. ESM1 immunostaining behind the angiogenic front was greatly reduced in *Dll4* $^{iΔEC/ΔEC}$ *NICD* $^{iOEC/OEC}$ double mutant retinas (arrows).

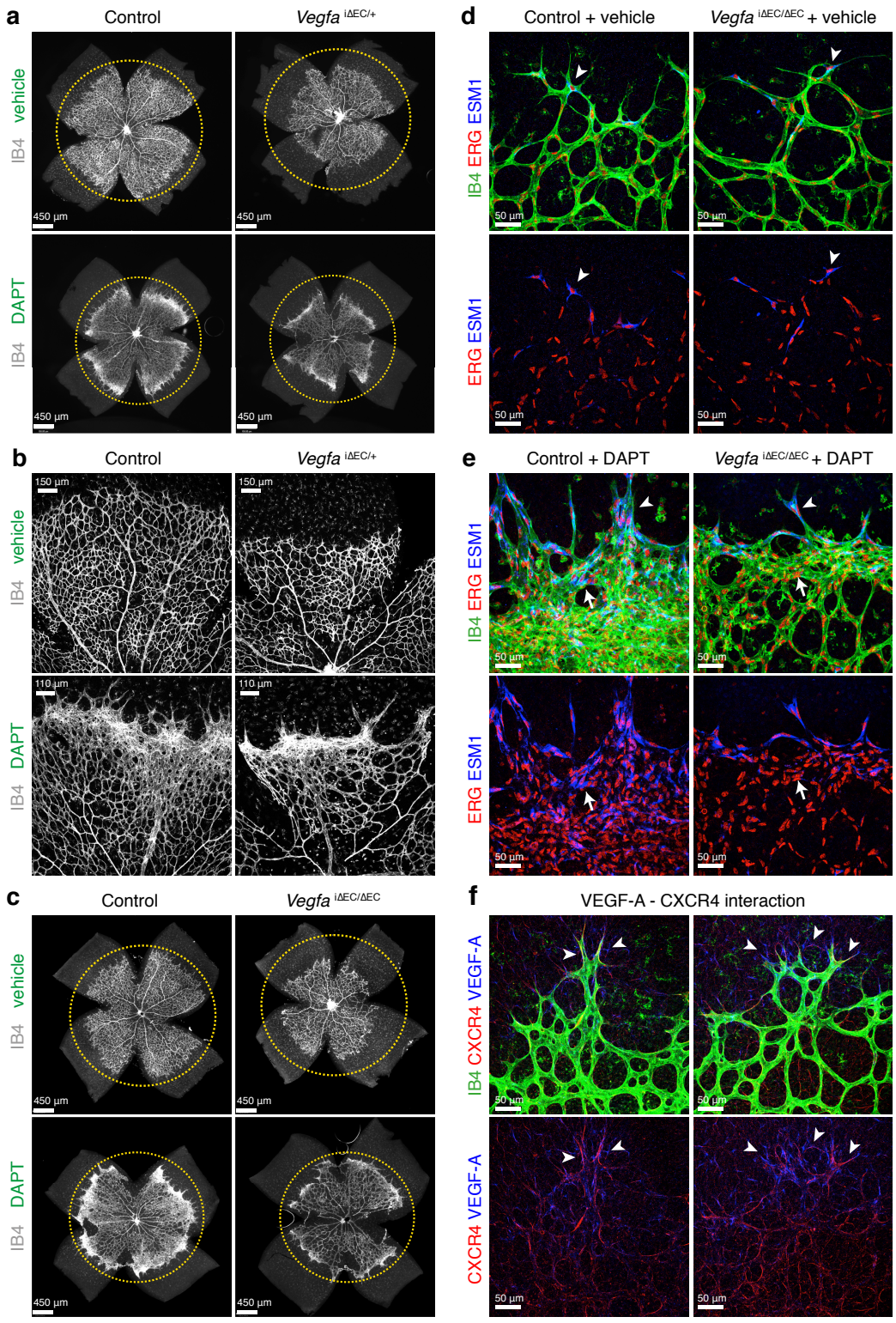


**Supplementary Figure 2** Endothelial VEGF signalling in Notch-dependent angiogenesis **a**, **b**, Representative overview (**a**) and confocal images (**b**) of IB4-stained *Vegfa* $^{i\Delta EC/+}$ and control retinas treated with vehicle or with DAPT. Circles indicate vessel outgrowth in control. **c**, Representative overview pictures of IB4-stained *Vegfa* $^{i\Delta EC/\Delta EC}$ and control retinas treated with vehicle or with DAPT. Circles indicate vessel outgrowth in control. **d**, **e**, Confocal images of IB4 (green), ESM1 (blue) and ERG (red) stained vehicle (**d**) and DAPT-treated (**e**) *Vegfa* $^{i\Delta EC/\Delta EC}$ and control P6 retinas. Note residual ESM1 staining (arrowheads) in *Vegfa* $^{i\Delta EC/\Delta EC}$ EC sprouts but impaired DAPT-induced upregulation in the plexus (arrows) relative to control. **f**, Confocal images of IB4 (green), VEGF-A (blue) and CXCR4 (red) staining of P6 retina. Note correlation (arrowheads) between CXCR4 and VEGF-A immunosignals.

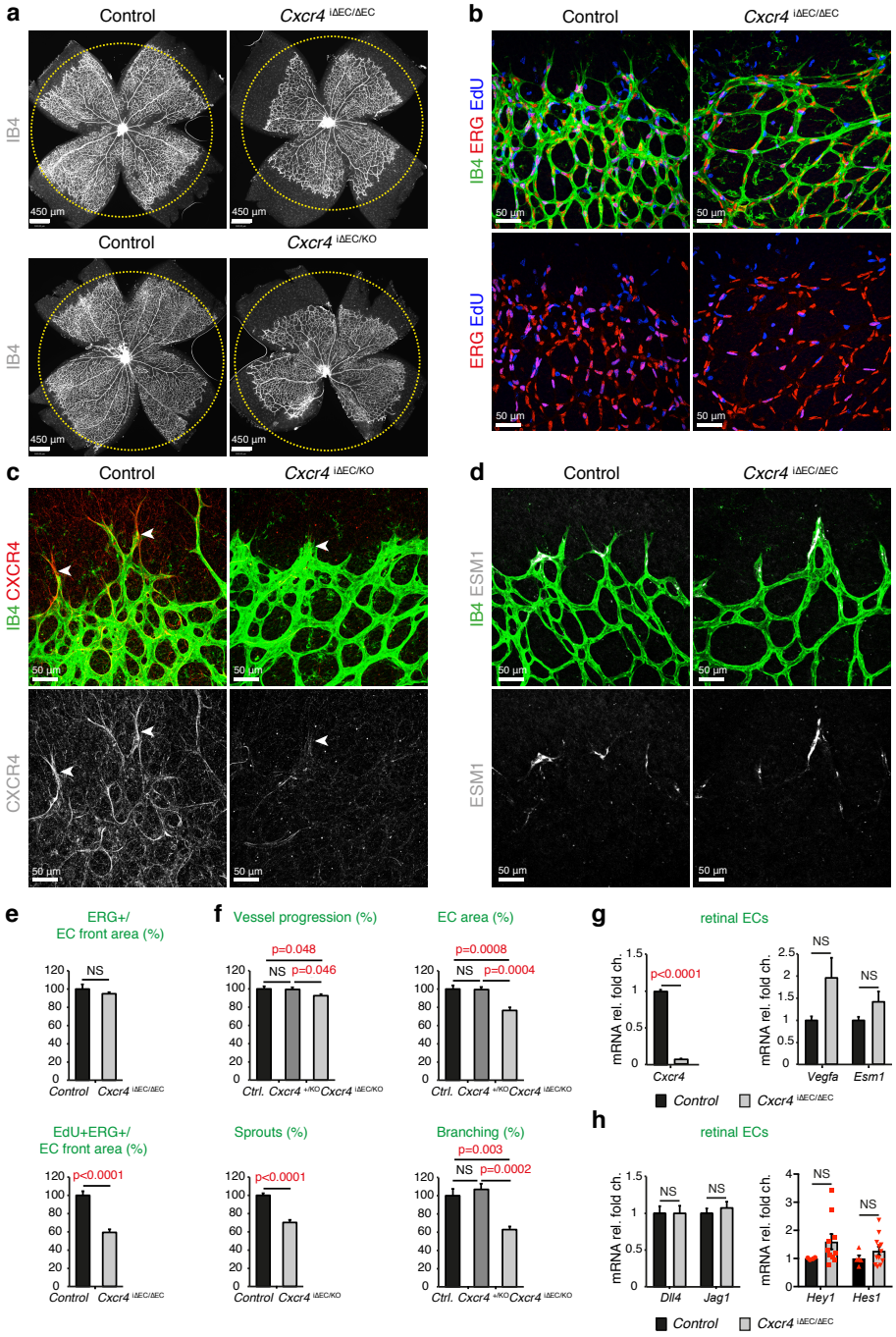


**Supplementary Figure 3** Role of endothelial CXCR4 in retinal angiogenesis **a**, Representative overview confocal images showing IB4-labelled *Cxcr4* $^{i\Delta EC/\Delta EC}$ and *Cxcr4* $^{i\Delta EC/KO}$ retinas together with the corresponding controls. Circles indicate vessel outgrowth in the control. **b**, Combined ERG (EC nuclei; red), IB4 (green) and EdU (blue) staining shows reduced ERG+ EdU+ EC numbers in *Cxcr4* $^{i\Delta EC/\Delta EC}$ retinal vessels compared to littermate control. EdU pulse-labelling was done 2h prior to analysis. **c**, Representative confocal images of CXCR4 (red/white) and IB4 (green) stained *Cxcr4* $^{i\Delta EC/KO}$ and control retinas. Arrowheads mark sprouts at the angiogenic front. **d**, ESM1 (white) and IB4 (green) staining of *Cxcr4* $^{i\Delta EC/\Delta EC}$ and control retinas. ESM1 expression is not overtly changed. **e**, Quantitative analysis of EC proliferation for *Cxcr4* $^{i\Delta EC/\Delta EC}$ and control littermates (n=7 control and 8 *Cxcr4* $^{i\Delta EC/\Delta EC}$ retinas from two independent tamoxifen injections). Graphs indicate reduction of *Cxcr4* $^{i\Delta EC/\Delta EC}$ ERG+ EdU+ cells per EC area at the angiogenic front relative to control, while the number of ERG+ cells was not significantly changed because of the impaired outgrowth. Data represent mean ± s.e.m. *P* values, two-tailed unpaired *t*-test. **f**, Quantitative analysis of vascular parameters for *Cxcr4* $^{i\Delta EC/KO}$, *Cxcr4* $^{KO/+}$ and control retinas: retinal vessel progression, EC area, branching points (n=7 control, 10 *Cxcr4* $^{KO/+}$ and 6 *Cxcr4* $^{i\Delta EC/KO}$ retinas), and sprouts (n=5 control and 6 *Cxcr4* $^{i\Delta EC/KO}$ retinas). Note absence of significant differences between *Cxcr4* $^{KO/+}$ heterozygotes and controls. Data represent mean ± s.e.m. *P* values, two-tailed unpaired *t*-test and one-way ANOVA with Tukey's multiple comparison post-hoc test. **g**, RT-qPCR analysis for *Cxcr4* (n=6 control and 7 *Cxcr4* $^{i\Delta EC/\Delta EC}$ mice), *Vegfa* (n=6 control and 12 *Cxcr4* $^{i\Delta EC/\Delta EC}$ mice) and *Esm1* (n=5 control and 7 *Cxcr4* $^{i\Delta EC/\Delta EC}$ mice) in sorted *Cxcr4* $^{i\Delta EC/\Delta EC}$ and control retinal ECs. Data represent mean ± s.e.m. *P* values, two-tailed unpaired *t*-test. **h**, RT-qPCR expression analysis of the Notch pathway components *Dll4* (n=7 control and 9 *Cxcr4* $^{i\Delta EC/\Delta EC}$ mice), *Jag1* (n=8 control and 12 *Cxcr4* $^{i\Delta EC/\Delta EC}$ mice) *Hey1* (n=4 control and 10 *Cxcr4* $^{i\Delta EC/\Delta EC}$ mice) and *Hes1* (n=5 control and 12 *Cxcr4* $^{i\Delta EC/\Delta EC}$ mice) in sorted *Cxcr4* $^{i\Delta EC/\Delta EC}$ and control retinal ECs. Data represent mean ± s.e.m. *P* values, two-tailed unpaired *t*-test.

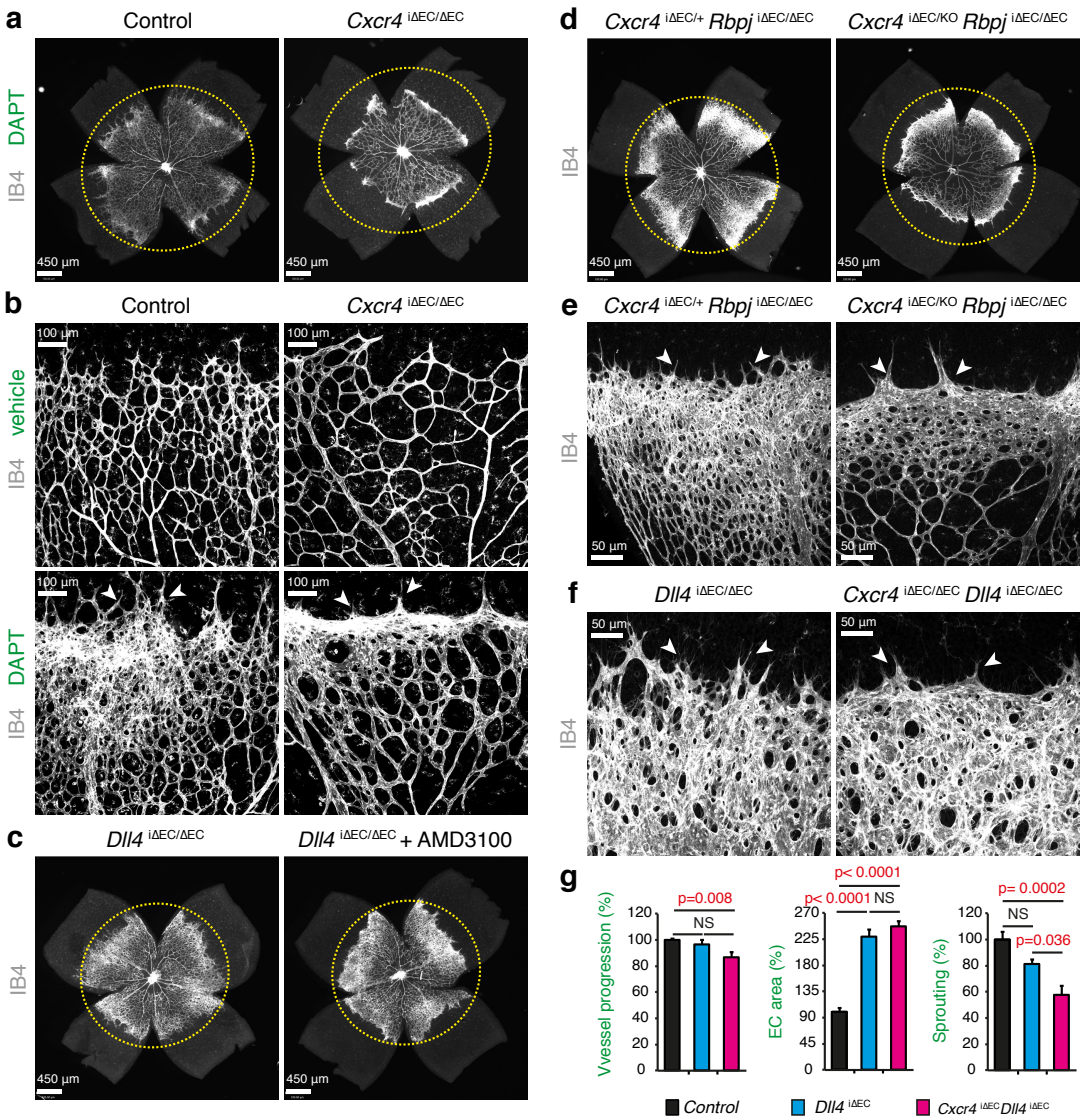


**Supplementary Figure 4** Role of CXCR4 in Notch-controlled angiogenesis **a**, Representative overview images showing DAPT-treated *Cxcr4* $^{i\Delta EC/\Delta EC}$ and control retinas. Circles indicate vessel outgrowth in control. **b**, Confocal images showing vehicle- or DAPT-treated *Cxcr4* $^{i\Delta EC/\Delta EC}$ and control retinas. Note the decrease sprouting (arrowheads) in DAPT-treated *Cxcr4* $^{i\Delta EC/\Delta EC}$ compared to control littermates. **c**, Overview images of IB4-stained untreated or AMD3100-treated *Dll4* $^{i\Delta EC/\Delta EC}$ retinas. Circles indicate vessel outgrowth in control. **d**, **e**, Representative overview pictures (**d**) and high magnification confocal images (**e**) of IB4-stained *Cxcr4* $^{i\Delta EC/KO}$ *Rbpj* $^{i\Delta EC/\Delta EC}$ and *Cxcr4* $^{i\Delta EC/+}$ *Rbpj* $^{i\Delta EC/\Delta EC}$ retinas. Sprouting (arrowheads) was reduced in *Cxcr4* $^{i\Delta EC/KO}$ *Rbpj* $^{i\Delta EC/\Delta EC}$ retinas compared to *Cxcr4* $^{i\Delta EC/+}$ *Rbpj* $^{i\Delta EC/\Delta EC}$ control retinas. **f**, Representative confocal images of IB4-stained *Cxcr4* $^{i\Delta EC/\Delta EC}$ *Dll4* $^{i\Delta EC/\Delta EC}$ and *Dll4* $^{i\Delta EC/\Delta EC}$ retinas. Sprouting (arrowheads) was reduced in *Cxcr4* $^{i\Delta EC/\Delta EC}$ *Dll4* $^{i\Delta EC/\Delta EC}$ retinas relative to *Dll4* $^{i\Delta EC/\Delta EC}$ control retinas. **g**, Quantitative analysis of vascular parameters for *Cxcr4* $^{i\Delta EC/\Delta EC}$ *Dll4* $^{i\Delta EC/\Delta EC}$, *Dll4* $^{i\Delta EC/\Delta EC}$ and control (Cre negative) retinas: retinal vessel progression, EC area and sprouting (n=8 control, 6 *Dll4* $^{i\Delta EC/\Delta EC}$ and 6 *Cxcr4* $^{i\Delta EC/\Delta EC}$ *Dll4* $^{i\Delta EC/\Delta EC}$ retinas). Note significant differences in sprouting but not in vessel progression and EC area between *Cxcr4* $^{i\Delta EC/\Delta EC}$ *Dll4* $^{i\Delta EC/\Delta EC}$ and *Dll4* $^{i\Delta EC/\Delta EC}$ retinas. Data represent mean ± s.e.m. *P* values, one-way ANOVA with Tukey's multiple comparison post-hoc test.

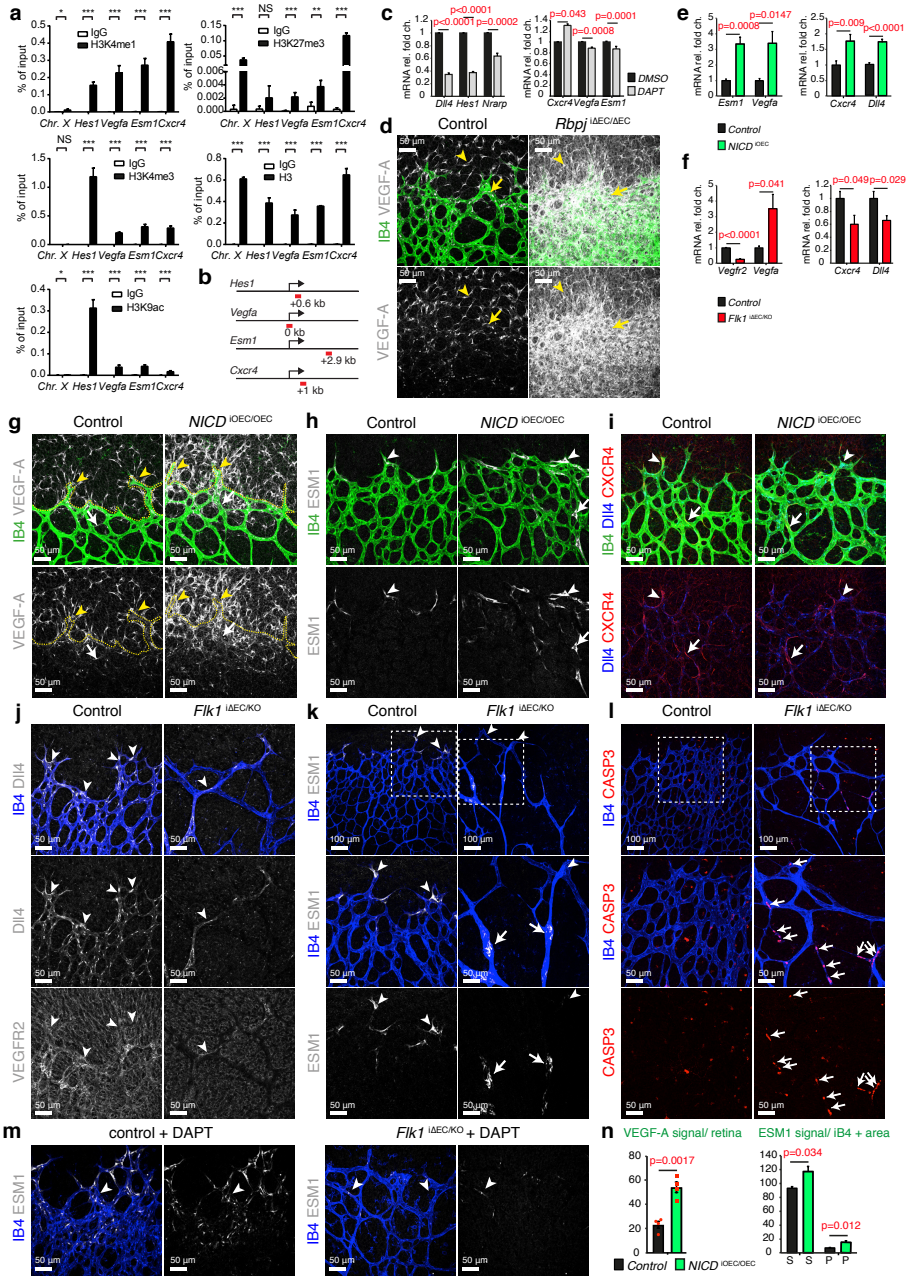


**Supplementary Figure 5** Notch and VEGF-A-controlled processes **a**, ChIP analysis of modified and total H3 at the *Hes1, Vegfa, Esm1* and *Cxcr4* loci in MS1 cells. A region located on chromosome X (*Chr. X*) was used as control. Shown is mean ± SD of 3 independent experiments for H3K4me1, H3K4me3 and total H3 and 2 independent experiments, measured twice each, for H3K9ac and H3K27me3 ([NS] not significant, [*] $P < 0.05$, [**] $P < 0.01$, [***] $P < 0.001$, two-tailed unpaired *t*-test). Statistics source data for are shown in Supplementary Table 3. **b**, Representation of regions (red) analysed by ChIP with distance in kilobases (kb) relative to transcriptional start sites (black arrows). **c**, RT-qPCR analysis of the indicated genes in MS1 cells treated with DMSO or DAPT for 3h (n=6 DMSO-treated MS1 and 6 DAPT-treated MS1; individual experiments in triplicate). Data represent mean ± s.e.m. *P* values, two-tailed unpaired *t*-test. **d**, Elevated VEGF-A (white) in the P7 *Rbpj* $^{i\Delta EC/\Delta EC}$ vascular plexus (arrows) and adjacent avascular tissue (arrowheads). Images are representative of three mice analysed. **e**, RT-qPCR analysis of *Esm1* (n=6 control and 8 *NICD* $^{iOEC/OEC}$ mice), *Vegfa* (n=5 control and 9 *NICD* $^{iOEC/OEC}$ mice), *Cxcr4* (n=6 control and 10 *NICD* $^{iOEC/OEC}$ mice) and *Dll4* (n=6 control and 9 *NICD* $^{iOEC/OEC}$ mice) in sorted *NICD* $^{iOEC/OEC}$ and control retinal ECs. Data represent mean ± s.e.m. *P* values, two-tailed unpaired *t*-test. **f**, RT-qPCR analysis of *Vegfr2* (n=6 control and 10 *Flk1* $^{i\Delta EC/KO}$ mice), *Vegfa* (n=6 control and 6 *Flk1* $^{i\Delta EC/KO}$ mice), *Cxcr4* (n=6 control and 6 *Flk1* $^{i\Delta EC/KO}$ mice) and *Dll4* (n=7 control and 5 *Flk1* $^{i\Delta EC/KO}$ mice) in sorted *Flk1* $^{i\Delta EC/KO}$ and control ECs. Data represent mean ± s.e.m. *P* values, two-tailed unpaired *t*-test. **g**, Upregulation of VEGF-A (white) in P6 *NICD* $^{iOEC/OEC}$ ECs (white arrows) and avascular retina (yellow arrowheads). **h**, Increased expression of ESM1 (white) in *NICD* $^{iOEC/OEC}$ sprouts (arrowheads) and plexus (arrows). **i**, Increased expression of Dll4 (blue) in *NICD* $^{iOEC/OEC}$ capillaries, whereas CXCR4 (red) did not overtly change in mutant sprouts (arrowheads) and plexus (arrows). **j**, Downregulation of VEGFR2 and Dll4 in *Flk1* $^{i\Delta EC/KO}$ vessels with some residual signal (arrowheads). **k**, Lost ESM1 (white) staining in *Flk1* $^{i\Delta EC/KO}$ sprouts (arrowheads) and ectopic plexus expression (arrows). Panels in centre and bottom rows show higher magnifications and ESM1 signal of insets. **l**, Cleaved caspase 3 (CASP3; red) detects EC death (arrows) in *Flk1* $^{i\Delta EC/KO}$ retinal vessels. Panels in centre and bottom rows show higher magnifications and CASP3 signal of insets. **m**, DAPT-induced ESM1 (white) expression in control (arrowheads) but not in *Flk1* $^{i\Delta EC/KO}$ vascular plexus. **n**, Quantitation of VEGF-A in P6 total retina (n=4 control and 4 *NICD* $^{iOEC/OEC}$ retinas) and ESM1 in IB4+ vessels sprouts (S) and plexus (P) (n=5 control and 5 *NICD* $^{iOEC/OEC}$ retinas).

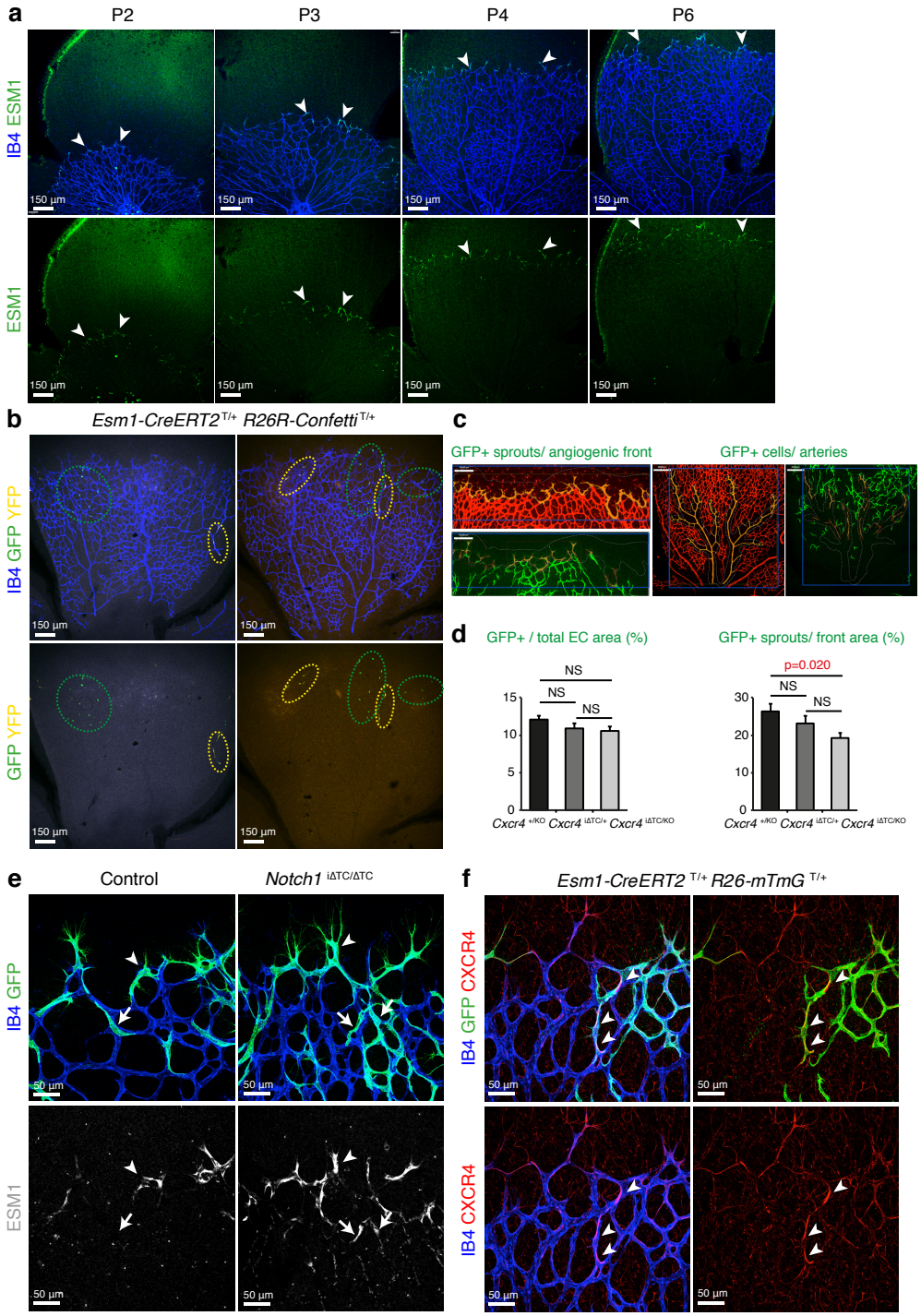


**Supplementary Figure 6** Genetic tracking and manipulation of tip cells *in vivo* **a**, Confocal images of IB4 (blue) and ESM1 (green) stained retinas at the indicated postnatal stages. Note continuous presence of ESM1 in angiogenic sprouts. **b**, Examples of clonal expansion of recombined ECs in *Esm1-CreERT2* $^{T/+}$ *R26R-Confetti* $^{T/+}$ double transgenics. IB4 labels ECs (blue), while nuclear GFP and cytoplasmic YFP mark recombined cell clones in arteries or at the angiogenic front (encircled areas ECs). **c**, Example of quantitation approach used to analyse the percentage of recombined GFP+ sprout area (green; orange in bottom image) per total angiogenic front area (orange in top image) and to analyse the percentage of recombined GFP+ cells in arteries (green; orange in right image) per total arterial EC area (orange in left image). **d**, Quantitation of *Cxcr4* $^{iΔTC/KO}$, *Cxcr4* $^{iΔTC/+}$ and *Cxcr4* $^{+/KO}$ GFP+ cells per total endothelial area (n=10 *Cxcr4* $^{+/KO}$, 10 *Cxcr4* $^{iΔTC/+}$ and 8 *Cxcr4* $^{iΔTC/KO}$ retinas) and of GFP+ sprouts per front area (n=10 *Cxcr4* $^{+/KO}$, 10 *Cxcr4* $^{iΔTC/+}$ and 8 *Cxcr4* $^{iΔTC/KO}$ retinas) at 96h after 4-OHT injection. Data represent mean ± s.e.m. *P* values, two-tailed unpaired *t*-test. **e**, Confocal images of IB4 (blue), GFP (green) and ESM1 (white) staining in P6 *Notch1* $^{iΔTC/ΔTC}$ (*Esm1-CreERT2* $^{T/+}$ *Notch1* $^{loxlox}$ *R26-mTmG* $^{T/+}$) and control (*Esm1-CreERT2* $^{T/+}$ *R26-mTmG* $^{T/+}$) retinas at 96h after 4-OHT injection. Note presence of ESM1 immunosignal in GFP+ *Notch1* $^{iΔTC/ΔTC}$ tip cells (arrowheads) and capillaries (arrows). **f**, IB4 (blue), GFP (green) and CXCR4 (red) staining of *Esm1-CreERT2* $^{T/+}$ *R26-mTmG* $^{T/+}$ retinas at 96h after 4-OHT injection. Recombined GFP+ cells found within the plexus area (arrowheads) are positive for CXCR4.

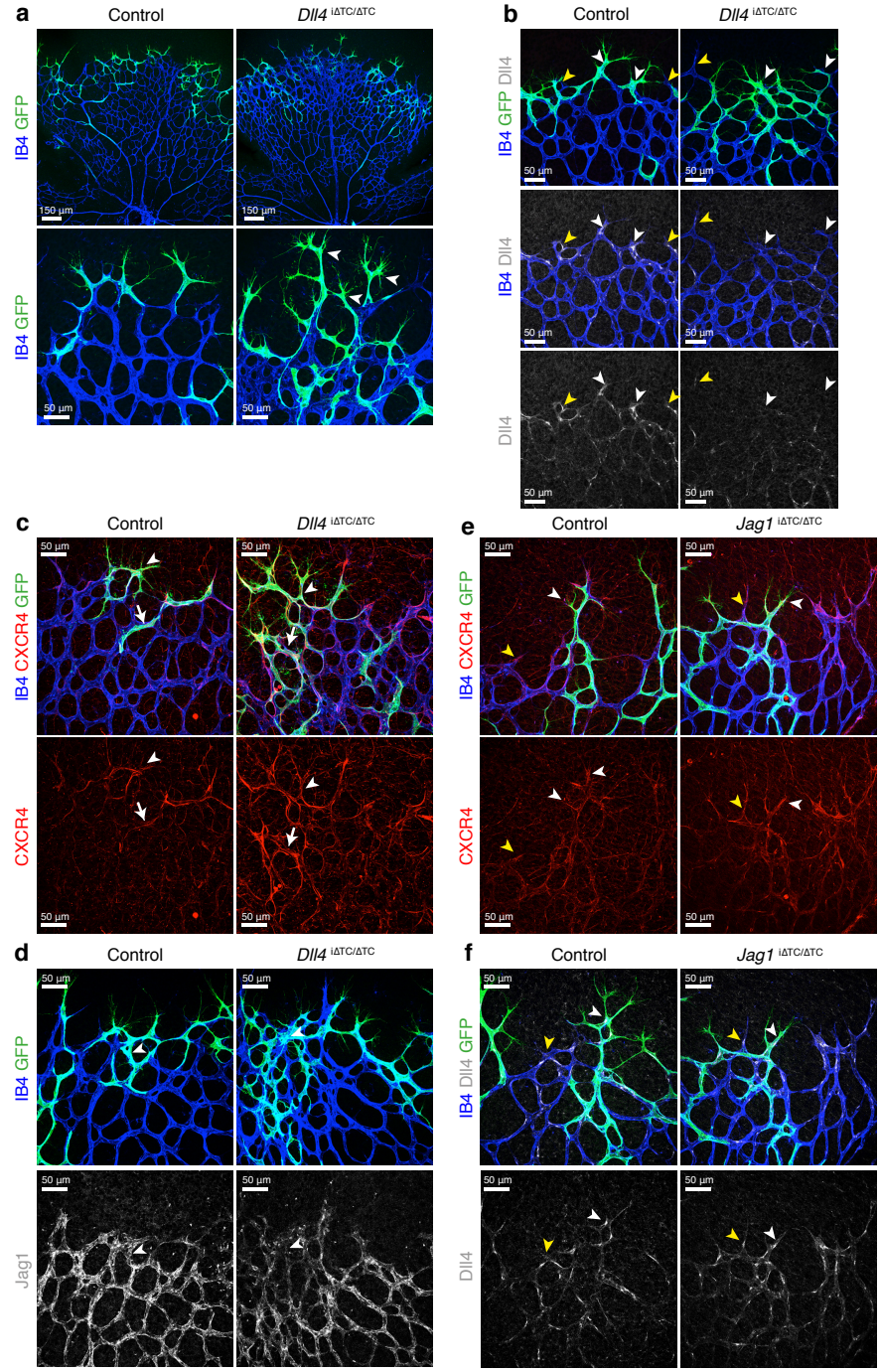


**Supplementary Figure 7** Control of tip cell behaviour by Dll4 and Jag1 **a**, Representative overview and high magnification confocal images of GFP-labelled (green) *Dll4* $^{iΔTC/ΔTC}$ (*Esm1-CreERT2* $^{T/+}$ *Dll4* $^{loxlox}$ *R26-mTmG* $^{T/+}$) and control (*Esm1-CreERT2* $^{T/+}$ *R26-mTmG* $^{T/+}$) ECs in the retinal vasculature (IB4, blue) at 48h after 4-OHT administration. Arrowheads indicate Dll4-deficient GFP+ tip cells displaying increased extension of protrusions and filopodia. **b**, Confocal images of IB4 (blue), GFP (green) and Dll4 (white) staining in P6 *Dll4* $^{iΔTC/ΔTC}$ and control retinas at 96h after 4-OHT injection. Note absence of Dll4 immunosignal in GFP+ *Dll4* $^{iΔTC/ΔTC}$ tip cells ECs (white arrowheads) and reduced expression of Dll4 in non-recombined ECs (yellow arrowheads). **c**, IB4 (blue), GFP (green) and CXCR4 (red) staining in P6 *Dll4* $^{iΔTC/ΔTC}$ and control retinas at 96h after 4-OHT injection. Note increased CXCR4 immunosignal in GFP+ *Dll4* $^{iΔTC/ΔTC}$ cells in plexus area (arrows) but not in sprouts (arrowheads) as compared to control GFP+ cells. **d**, IB4 (blue), GFP (green) and Jag1 (white) staining in P6 *Dll4* $^{iΔTC/ΔTC}$ and control retinas at 96h after 4-OHT injection. Note reduced Jag1 expression in GFP+ *Dll4* $^{iΔTC/ΔTC}$ cells plexus area (arrowheads) as compared to control GFP+ cells. **e**, Confocal images of IB4 (blue), GFP (green) and CXCR4 (red) staining in P6 *Jag1* $^{iΔTC/ΔTC}$ (*Esm1-CreERT2* $^{T/+}$ *Jag1* $^{loxlox}$ *R26-mTmG* $^{T/+}$) and control (*Esm1-CreERT2* $^{T/+}$ *R26-mTmG* $^{T/+}$) retinas at 96h after 4-OHT injection. Note no significant difference for CXCR4 immunosignal between *Jag1* $^{iΔTC/ΔTC}$ recombined sprouts (white arrowheads) and non-recombined tip cells (yellow arrowheads). **f**, IB4 (blue), GFP (green) and Dll4 (white) staining in P6 *Jag1* $^{iΔTC/ΔTC}$ and control retinas at 96h after 4-OHT injection. Note no obvious difference for Dll4 immunosignal between *Jag1* $^{iΔTC/ΔTC}$ recombined sprouts (white arrowheads) and non-recombined tip cells (yellow arrowheads). Images in **a**-**f** are representative of three mice analysed.

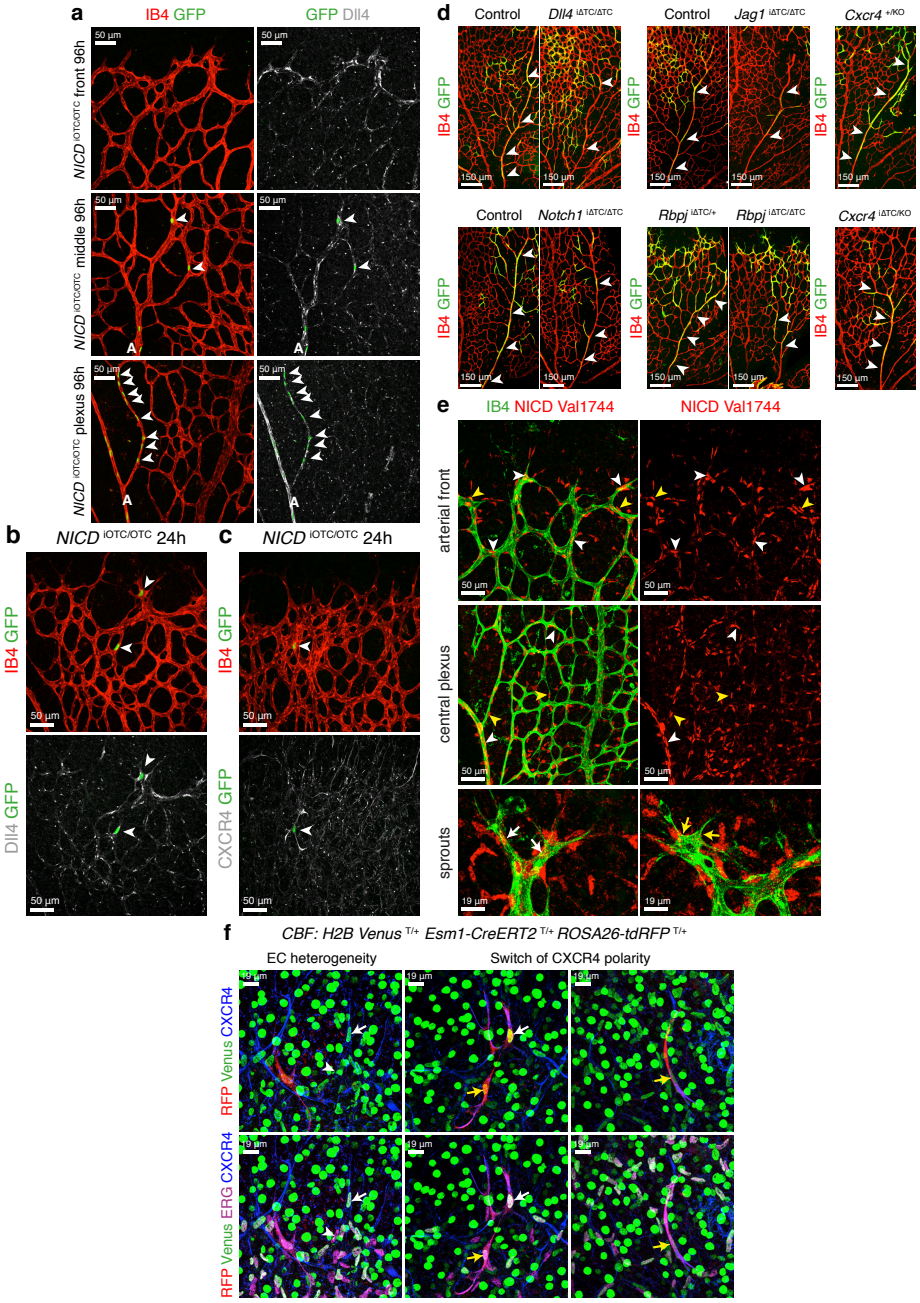


**Supplementary Figure 8** Notch activation directs tip cell progeny into arteries **a**, Maximum intensity projection of IB4 (red), Dll4 (white) and NICD (GFP, green) staining in *NICD* $^{iOTC/OTC}$ retinas at 96h after 4-OHT administration. Arrowheads mark recombined nuclear GFP+ cells; arteries (A) are indicated. Arrowheads indicate GFP+ ECs with Dll4 immunostaining in and around arteries (top panels). Images are representative of two mice analysed. **b**, **c**, Confocal images showing IB4 (red), NICD (GFP, green) and Dll4 (white) (**b**) or CXCR4 (white) (**c**) staining in *NICD* $^{iOTC/OTC}$ retinas at 24h after 4-OHT administration. Arrowheads mark recombined GFP+ ECs with Dll4 (**b**) and CXCR4 (**c**) immunosignal in capillaries at or near the angiogenic front. Whereas all *NICD* $^{iOTC/OTC}$-expressing cells from three mice analysed express Dll4, only 72% of *NICD* $^{iOTC/OTC}$-expressing cells from three mice analysed show CXCR4 immunostaining. **d**, Representative images showing arterial incorporation of recombined GFP+ cells in *Dll4* $^{iΔTC/ΔTC}$, *Jag1* $^{iΔTC/ΔTC}$, *Notch1* $^{iΔTC/ΔTC}$, *Rbpj* $^{iΔTC/ΔTC}$ and *Cxcr4* $^{iΔTC/KO}$ mice and their respective controls. Note reduced arterial contribution of GFP+ ECs in *Dll4* $^{iΔTC/ΔTC}$, *Jag1* $^{iΔTC/ΔTC}$ and *Notch1* $^{iΔTC/ΔTC}$ at 96h after 4-OHT injection. This phenotype was also seen in the *Rbpj* $^{iΔTC/ΔTC}$ at 72h but not in the *Cxcr4* $^{iΔTC/KO}$ vasculature at 96h after 4-OHT injection. Arrowheads point to GFP+ ECs incorporated into arteries. **e**, Whole-mount retina immunostaining of IB4 (green) and active NICD (NICD Val1744, red). Confocal images show the angiogenic growth front on top of the artery and central vascular plexus. NICD signal is detected in ECs (white arrowheads) and perivascular cells (yellow arrowheads). High NICD signal decorates arteries and ECs in the peri-arterial plexus (bottom). Bottom row panels show examples of sprouting ECs without (yellow arrows) or with high active NICD (white arrows). **f**, Additional combinations of maximum intensity projections (same regions as in Figure **8d**) for CXCR4 (blue), ERG (purple), RFP (red, ESM1 recombined cells) and active endogenous Notch (YFP/Venus, green) immunostaining in *CBF:H2B Venus* Notch reporter (*Esm1-CreERT2* $^{T/+}$ *CBF:H2B Venus* $^{T/+}$ *ROSA26-tdRFP* $^{T/+}$). White arrows point to endothelial cells with high Notch activity, while white arrowheads indicate ERG+ cells with no Notch activity. Yellow arrows indicate ERG+ endothelial cells from capillary front, with detectable Notch activity and reversed CXCR4 polarization.

**Supplementary Table Legends**

**Supplementary Table 1** Information on antibodies used in this study **a**, **b**, Tables indicate primary and secondary antibodies used for whole-mount immunostaining of mouse retinas. **c**, The table shows details of fluorophore-conjugated primary antibodies used for fluorescence-activated sorting (FACS) of mouse retinal cells. **d**, The table indicates antibodies used for chromatin immunoprecipitation (ChIP) experiments.

**Supplementary Table 2** Primer pair and probe sequences for quantitative reverse transcription polymerase chain reaction **a**, The table lists the catalogue numbers and probe types of Applied Biosystem Taqmans used for RT-qPCR of sorted mouse retinal endothelial cells. **b**, The table shows self-designed primer pairs and probes used for transcript detection of encoded VEGF-A isoforms by RT-qPCR of whole mouse retinas. **c**, The table indicates the primer pairs and probes used for ChIP experiments.

**Supplementary Table 3** Statistics Source Data The table provides the qPCR source data of chromatin immunoprecipitation (ChIP) assays from Figure 5b, c and Supplementary Figure 5a.